Journal of African Earth Sciences 207 (2023) 105049

Contents lists available at ScienceDirect

Journal of African Earth Sciences

journal homepage: www.elsevier.com/locate/jafrearsci

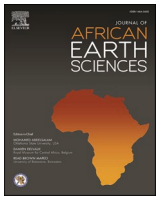

# Characterisation and rare-metal potential of the Winneba-Mankoadze pegmatites, Southern Ghana: Evidence of two pegmatite fields

Salaam Jansbaka Adams [a,b], Marieke Van Lichtervelde [c], Prince Ofori Amponsah [d,*], Prosper Mackenzie Nude [d], Daniel Kwadwo Asiedu [d], Samuel Boakye Dampare [a,e]

[a] School of Nuclear and Allied Sciences, College of Basic and Applied Sciences, University of Ghana, P.O. Box LG 80, Legon – Accra, Ghana
[b] School of Natural and Environmental Sciences, University of Environment and Sustainable Development, PMB - Somanya, Ghana
[c] GET, Univ Toulouse, CNRS, UPS, IRD, 14 Avenue Edouard Belin, 31400, Toulouse, France
[d] Department of Earth Science, College of Basic Applied Sciences, University of Ghana, P. O. Box LG 58, Legon – Accra, Ghana
[e] Ghana Atomic Energy Commission, P.O. Box LG 80, Legon – Accra, Ghana

ARTICLE INFO

Handling Editor: M Mapeo

*Keywords:*
Rare-element pegmatites
Spodumene
Columbite-group minerals
Extreme fractionation

ABSTRACT

In southern Ghana, the region along the coast between Accra and Cape Coast hosts a large number of pegmatites mineralized in lithium, niobium-tantalum and tin. The pegmatites occur in many distinct groups, each extending over several kilometers. They intrude metasedimentary units of the Birimian Supergroup, and are associated with early to late orogenic granite intrusions which are metaluminous, sterile, and too old to be potential parental granites for the pegmatites. In this study, we characterized the Winneba-Mankoadze group of geographically coeval pegmatites, using field description, petrography, rare-metal mineralogy and accessory mineral geochemistry on micas, garnet and Nb–Ta–Sn minerals, in order to determine its rare-metal potential and to investigate its origin. The results indicate that the pegmatites are part of the albite-spodumene type of the Lithium–Cesium–Tantalum (LCT) family. The rare metal mineral assemblages are particularly complex and display relevant oxide species such as columbite- and wodginite-group minerals, tapiolite, microlite, cassiterite and rutile, which are evidences of an extremely evolved magmatic system. Based on mineral assemblages, whole-rock geochemistry, and mineral geochemistry on garnet, micas and the CGM, two pegmatite fields are distinguished in the Winneba-Mankoadze group, and an anatectic origin is proposed. For the first time in West Africa, we fully describe a highly fractionated LCT-family pegmatite field comparable to the most evolved pegmatite bodies in the world.

## 1. Introduction

Rare-element pegmatites host world-class deposits of rare elements such as Li, Cs, Ta, Nb, Sn, Be, U, and Th (Černý, 1991; Thomas and Davidson, 2007; Linnen et al., 2012; Dill, 2015). Reserves of these metals are documented on the African continent (Von Knorring and Condliffe, 1987; Fetherston, 2004; Melcher et al., 2008, 2015), the most economic being associated with ancient cratons: the Kasai-Congo craton in Central Africa, the Kapvaal craton in southern Africa, and the West African craton (Melcher et al., 2008, 2015). The deposits are distributed in five metallogenic periods; Archean >2500 Ma, Paleoproterozoic ~2000 Ma, Neoproterozoic ~1000 Ma, Pan African ~500 Ma and Mesozoic ~200 Ma (Melcher et al., 2015).

West Africa hosts important rare-metal deposits, e.g., in Ghana, Nigeria, Ivory Coast, Mali and Senegal (Agomor, 1987; Ndiaye et al., 1997; Allou, 2005; Allou et al., 2005; Dampare et al., 2005; Nude et al., 2011; Adams, 2013; Wilde et al., 2021; Bonzi et al., 2022). In Ghana, rare-metal deposits occur in three main areas: (i) Akim-Oda and Anamase prospects, 100 km northwest of Accra; (ii) Winneba District and the Makuba Lagoon, southern Ghana; (iii) Cape Coast to Saltpond coastline, southern Ghana (Agomor, 1987; Chalokwu et al., 1997; Dampare et al., 2005; Nude et al., 2011; Adams, 2013). Many pegmatites have also been documented in the Bole-Nangodi belt, although their metallogenic significance is as yet unknown.

In general, very few studies, mainly geological and/or geochemical, have been carried out on the Ghanaian pegmatites (Kesse, 1985; Agomor, 1987; Chalokwu et al., 1997; Nude et al., 2011). The only existing works that describe their mineralization are those of Adams (2013) in

* Corresponding author.
*E-mail address:* pamponsah@ug.edu.gh (P.O. Amponsah).

https://doi.org/10.1016/j.jafrearsci.2023.105049
Received 9 June 2023; Received in revised form 28 August 2023; Accepted 30 August 2023
Available online 31 August 2023
1464-343X/

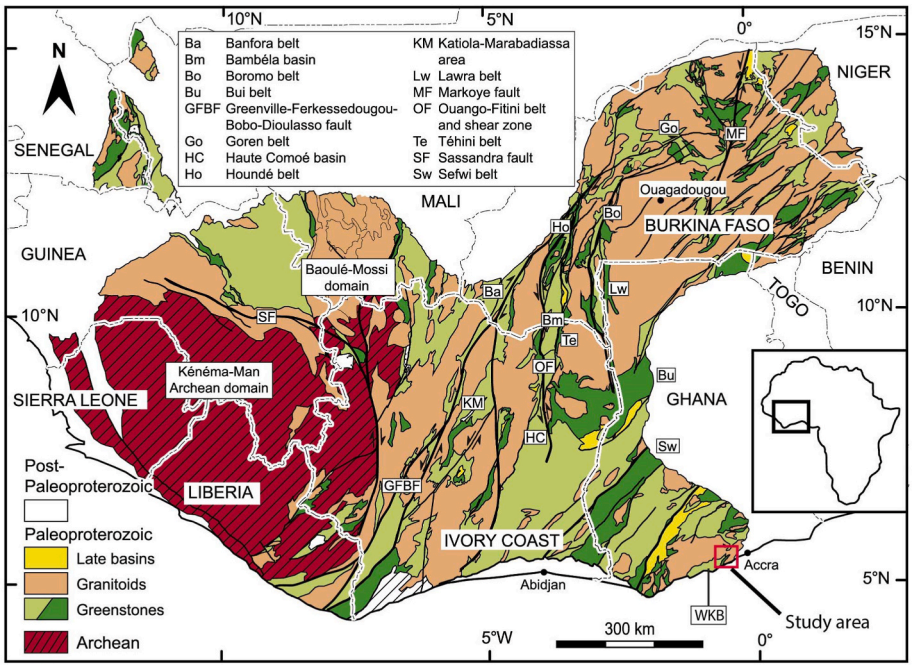


**Fig. 1.** The Leo Man Rise showing the Paleoproterozoic Birimian Supergroup of Ghana. WKB = Winneba-Kibi belt. Modified after Milesi et al. (2004).

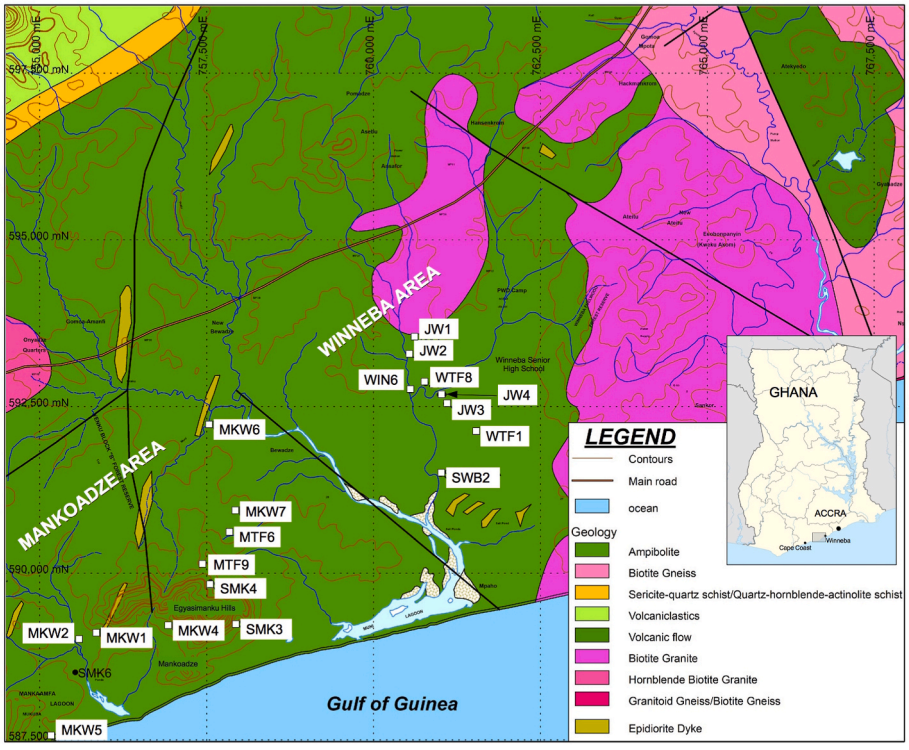


**Fig. 2.** Lithological map of the Winneba-Mankoadze area with location of the studied pegmatite outcrops (listed in first column of Table 1).

the Winneba-Mankoadze area, and Dampare et al. (2005) in the Akim Oda area, the latter being associated with important coltan placer deposits that were artisanally mined in the past. A resurgence of interest in rare metals and, in particular, lithium in the subregion calls for a better understanding of the origin and magmatic evolution of these pegmatite deposits. This paper seeks to establish the petrography, mineralogy, and rare-metal mineralization of the Winneba-Mankoadze pegmatites. It also seeks to use geochemical data on Nb–Ta-bearing minerals, the micas, and garnet to constrain the fractionation of the pegmatite-forming melts and to discuss their granite-related versus anatectic origin.

## 2. Geological settings

Winneba-Mankoadze is located within the Birimian Supergroup of Ghana (2195-2072 Ma) (Agyei-Duodu et al., 2009), which is part of the Leo-Man Rise that forms the southernmost part of the West African

**Table 1**
GPS coordinates of the studied outcrops and petrological description of the samples. The projection used is WGS84 UTM zone 30N.

| | Outcrop name | Easting (mE) | Northing (mN) | Sample | Petrological hand sample description | Accessory minerals and Nb–Ta–Sn oxides | | | | | | | |
|---|---|---|---|---|---|---|---|---|---|---|---|---|---|
| | | | | | | CGM | WGM | Tap | Cst | Pcl | Zrn | Meta | Ilm |
| Mankwase | MKW1 | 755850 | 589120 | MKW1A | Aplitic Qz Ab Ms | X | X | X | | | X | X | |
| | | | | MKW1B | Greisen Ms replacing Qz Kfs | X | | | | X | X | X | |
| | MKW2 | 755770 | 588980 | MKW2A | Aplitic Qz Ab Ms | X | | | | X | X | X | |
| | | | | MKW2B | Aplitic Qz Ab Ms | X | | | | | X | X | |
| | MKW4 | 756930 | 589220 | MKW4A | Cleavelanditic Ab Qz; CG Tur Ap | X | X | X | X | | | | |
| | | | | MTF16 | Aplitic Qz Ab Ms Tur | X | | | X | | X | | |
| | MKW5 | 755310 | 587580 | MKW5A | Cleavelanditic Ab Qz Tur replacing Kfs | no thin section | | | | | | | |
| | | | | MKW5B | CG Ab Qz Kfd Ms | X | | | | X | X | | |
| | | | | MTF12 | CG Qz Kfs Ms Tur Brl | X | X | | X | | | X | |
| | MKW6 | 757540 | 592230 | MKW6B | CG Qz Kfd Ms Tur Ap | X | X | | X | X | X | X | |
| | MKW7 | 757930 | 590940 | MKW7B | Aplitic Qz Ab Ms; MG Grt | no thin section | | | | | | | |
| | | | | MTF2 | Greisen Ms replacing Qz Kfd Grt | X | X | | | | X | | |
| | | | | MTF3 | Aplitic Ab replacing CG Qz Fsp Ms Grt | X | X | | | | | X | |
| | | | | MTF4 | Aplitic Qz Ab Ms Tur Grt | | X | | | | X | | |
| | MTF6 | 757950 | 590610 | MTF6 | Aplitic Qz Ab Ms | X | X | | | | | | |
| | MTF9 | 757620 | 590040 | MTF9 | CG Ksp Qz Tur Grt | X | X | X | X | | X | X | |
| | | | | MTF11 | CG Qz Kfs Spd | | X | | X | | | X | |
| | SMK3 | 757940 | 589240 | SMK3 | Aplitic Qz Ab Tur; MG Ap | X | X | | | | X | | |
| | SMK4 | 757550 | 589820 | SMK4B | CG Qz Kfs Ms Tur | X | X | | X | | X | | |
| | | | | SMK4C | CG Qz Kfs Ms Tur Grt | X | X | | X | | | X | |
| Winneba | JW1 | 760600 | 593540 | WIN1A | CG Ab Qz | X | X | | | X | X | X | |
| | | | | WIN7 | CG Qz Fsp | no thin section | | | | | | | |
| | JW2 | 760520 | 593300 | WIN2A | Cleavelanditic Ab; CG Qz; FG Grt | X | | | | | | X | |
| | | | | WIN2B | CG Fsp Qz Grt replaced by FG Ab | X | | | | X | X | X | |
| | JW3 | 761100 | 592540 | WIN3A | CG Qz Kfs Ms Spd | no thin section | | | | | | | |
| | | | | WIN3B | CG Qz Kfs Ms Spd | X | | | | | | | |
| | | | | WTF3 | CG Qz Fsp Spd Ms | X | | | | | | | |
| | | | | WTF4 | CG Qz Fsp Spd | X | | | | X | X | | |
| | | | | WTF5 | CG Qz Fsp Spd Ap Ms Grt | X | | | | X | | | |
| | JW4 | 761050 | 592680 | WIN4A | CG Qz Fsp Spd Ms Grt | X | X | | | X | | | |
| | | | | WIN4B | CG Ab Qz Ms Grt | | | | | | | | |
| | | | | WIN4C | CG Qz Spd Ms Grt | X | X | | X | X | X | X | X |
| | WIN6 | 760780 | 592850 | WIN6A | CG Qz Fsp Ms Tur | | | | | | | | X |
| | | | | WIN6B | CG Qz Fsp Ms Tur | no thin section | | | | | | | |
| | WTF1 | 761500 | 592160 | WTF1 | CG Qz Fsp Ms Grt | X | | | X | X | X | X | |
| | WTF8 | 760740 | 592880 | WTF8 | CG Qz Fsp Tur Grt | X | | | | X | X | | |
| | SWB2 | 761000 | 591490 | SWB2 | | no thin section | | | | | | | |

Mineral abbreviations principally after Whitney and Evans (2010). FG, MG and CG = fine-, medium- and coarse-grained Ab, albite; Ap, apatite; Brl, beryl; CGM, columbite-group mineral; Fsp, feldspar; Grt, garnet; Ilm, ilmenite; Kfs, K-feldspar; Meta, metamict U–Th bearing unidentified phases; Ms, Muscovite; Qz, quartz; Spd, spodumene; Tap, tapiolite; Tur, tourmaline; WGM, wodginite-group minerals; Zrn, zircon.

Craton (Fig. 1). The Leo-Man Rise comprises an Archean nucleus, the 3.00–2.50 Ga Kénéma-Man domain to the west, and the juvenile Paleoproterozoic Baoulé-Mossi domain (Leo-Man Rise) to the east (Hirdes et al., 1992; Taylor et al., 1992; Block et al., 2016; Salvi et al., 2016; Asiedu et al., 2019; Sapah et al., 2021; Forson et al., 2023).

The Birimian Supergroup of Ghana is classified into two lithostratigraphic units consisting of meta-volcanic and meta-sedimentary groups, overlaid with the younger, arenaceous, and clastic Tarkwaian Group (Hirdes et al., 1992; Leube et al., 1990; Taylor et al., 1992; Amponsah, 2012). Intruded in the Birimian meta-sedimentary basins and meta-volcanic belts are syn- and late-kinematic, frequently peraluminous granitoids of the Eburnean Plutonic suite, which crystallized between 2195 and 2072 Ma as a result of partial melting of slightly older Birimian sediments (Leube et al., 1990; Hirdes et al., 1992; Taylor et al., 1992; Agyei-Duodu et al., 2009; Jessell et al., 2012; Sakyi et al., 2019; Feng et al., 2019).

The Eburnean tectonic event which started between 2120 Ma and 2115 Ma (Agyei-Duodu et al., 2009) affected the Birimian Supergroup (2195–2072 Ma) of Ghana leading to crustal shortening and regional metamorphism. This event folded and metamorphosed some previously-formed Paleoproterozoic rocks. Pegmatite emplacement marks the end of this Eburnean Plutonism, which ends at 2072 Ma (Leube et al., 1990; Hirdes et al., 1992; Taylor et al., 1992; Amponsah et al., 2015, 2016a, 2016b; Feng et al., 2016).

The Winneba-Mankoadze area is located within the Palaeoproterozoic Winneba-Kibi Meta-volcanic belt which is composed of basaltic flows, andesitic lavas, amphibolites, pyroclastics, and granite-diorite plutonic rocks (Yao and Robb, 1998; Anum et al., 2015; Forson et al., 2020; Nyame et al., 2021). The Winneba area consists of meta-sedimentary and meta-volcanic Birimian rocks (Fig. 2), which are both intruded by the Winneba granitoids, which has Archean continental signatures (Leube et al., 1990; Petersson et al., 2016, 2018). The granitoids are composed of two-mica granodiorites, biotite granites, hornblende-biotite granite, leucogranites, pegmatites, and migmatites, as well as gneissic biotite granites, and occur from the southwest to the northeast of Winneba (Leube et al., 1990; Hirdes et al., 1992; Anum et al., 2015; Petersson et al., 2016, 2018). The biotite granites and granodiorites are gray, with biotite as the main mafic mineral, medium-grained, and foliated. The foliated, porphyritic, equigranular biotite granodiorites range in color from pale pink to light gray. The major minerals are quartz, alkali feldspar, plagioclase and biotite with accessory pink garnet and greenish chlorite. (Hirdes et al., 1992; Anum et al., 2015).

Amphibolite, hornblende-biotite-quartz schist, and quartz-hornblende-actinolite schist are among the "greenstones" that make up the rocks of the Mankoadze area (Nyame et al., 2021). The granitoids that intrude these rocks, which trend NE-SW, contain hornblende, biotite, and related quartz and pegmatite veins. Along foliation planes that

**Table 2**
Trace element whole rock geochemistry of the pegmatite samples in ppm. Outcrop names are those shown in first column of Tables 1 and in Fig. 2.

| | Mankwase | | | | | | | | | | | | | | | Winneba | | | | | | | | | | |
|---|---|---|---|---|---|---|---|---|---|---|---|---|---|---|---|---|---|---|---|---|---|---|---|---|---|---|
| Outcrop | MKW2 | MKW4 | MKW6 | MKW7 | SMK3 | | | | | | | SMK4 | | | | JW1 | JW2 | | JW3 | | JW4 | | | WTF8 | | WIN6 |
| Sample | MKW2 | MKW4 | MKW6 | MKW7 | SMK3D | SMK3E | SMK3F | SMK3G | SMK3A | SMK3B | SMK3C | SMK4A1 | SMK4A2 | SMK4D | SMK4E | JW1 | JW2A | JW2C | JW3A | JW3B | JW4A | JW4B | JW4C | JW6A | JW6B | WIN6 |
| SiO2 | 43.62 | 44.92 | 45.21 | 48.62 | 46.47 | 52.79 | 43.73 | 46.32 | 44.72 | 45.14 | 46.28 | 51.00 | 66.76 | 48.64 | 55.58 | 45.37 | 49.82 | 48.25 | 49.89 | 55.11 | 50.96 | 45.80 | 45.83 | 47.18 | 51.95 | 42.67 |
| TiO2 | 0.08 | 0.00 | 0.00 | 0.00 | 0.01 | 0.01 | 0.01 | 0.00 | 0.00 | 0.01 | 0.01 | 0.02 | 0.03 | 0.01 | 0.01 | 0.00 | 0.00 | 0.01 | 0.01 | 0.00 | 0.00 | 0.00 | 0.00 | 0.02 | 0.02 | 0.00 |
| Al2O3 | 15.81 | 11.21 | 11.86 | 18.49 | 13.25 | 10.29 | 11.21 | 11.64 | 10.77 | 11.30 | 11.05 | 12.02 | 2.50 | 11.43 | 12.23 | 12.01 | 11.99 | 10.76 | 12.67 | 7.98 | 10.67 | 11.49 | 11.28 | 10.25 | 11.33 | 11.00 |
| Fe2O3 | 1.69 | 0.19 | 0.32 | 0.51 | 0.16 | 0.59 | 0.74 | 0.81 | 0.84 | 0.90 | 0.96 | 1.95 | 1.52 | 0.74 | 0.19 | 0.14 | 0.23 | 0.37 | 0.72 | 0.98 | 0.32 | 0.21 | 0.16 | 0.44 | 0.33 | 0.09 |
| P2O5 | 1.48 | 0.31 | 0.20 | 0.27 | 0.06 | 0.05 | 0.30 | 0.34 | 0.37 | 0.26 | 0.64 | 0.19 | 0.06 | 0.16 | 0.06 | 0.04 | 0.04 | 0.07 | 0.11 | 0.09 | 0.08 | 0.05 | 0.05 | 0.03 | 0.04 | 0.04 |
| K2O | 2.06 | 0.22 | 1.09 | 3.89 | 3.70 | 1.84 | 0.23 | 0.16 | 0.13 | 0.07 | 0.12 | 1.53 | 0.64 | 0.26 | 3.71 | 0.37 | 0.04 | 0.48 | 5.16 | 1.03 | 3.23 | 1.64 | 0.61 | 0.19 | 0.17 | 0.10 |
| Na2O | 1.73 | 3.66 | 3.06 | 2.36 | 3.35 | 2.68 | 3.20 | 3.51 | 3.45 | 3.14 | 3.28 | 2.53 | 0.31 | 3.80 | 0.72 | 3.55 | 4.14 | 2.96 | 1.58 | 1.52 | 2.47 | 2.51 | 3.12 | 2.92 | 3.26 | 3.16 |
| MnO | 0.03 | 0.02 | 0.04 | 0.04 | 0.01 | 0.01 | 0.04 | 0.03 | 0.04 | 0.04 | 0.06 | 0.05 | 0.03 | 0.06 | 0.02 | 0.01 | 0.02 | 0.10 | 0.03 | 0.03 | 0.07 | 0.03 | 0.03 | 0.02 | 0.01 | 0.00 |
| CaO | 1.47 | 0.33 | 0.27 | 0.35 | 0.28 | 0.31 | 0.31 | 0.33 | 0.38 | 0.32 | 0.68 | 0.20 | 0.03 | 0.17 | 0.03 | 0.54 | 0.20 | 0.21 | 0.32 | 0.38 | 0.52 | 0.20 | 0.24 | 0.88 | 0.90 | 0.52 |
| MgO | 0.68 | 0.75 | 0.65 | 0.60 | 0.56 | 0.65 | 0.71 | 0.76 | 0.68 | 0.80 | 0.57 | 0.84 | 0.82 | 0.74 | 0.95 | 0.62 | 0.78 | 0.79 | 0.83 | 0.80 | 0.80 | 0.69 | 0.47 | 0.76 | 0.80 | 0.49 |
| SO3 | 0.05 | 0.04 | 0.04 | 0.05 | 0.05 | 0.05 | 0.05 | 0.05 | 0.04 | 0.06 | 0.05 | 0.03 | 0.03 | 0.04 | 0.05 | 0.04 | 0.04 | 0.08 | 0.07 | 0.05 | 0.05 | 0.06 | 0.12 | 0.04 | 0.04 | 0.04 |
| Cl | 0.13 | 0.11 | 0.12 | 0.13 | 0.13 | 0.13 | 0.13 | 0.12 | 0.13 | 0.12 | 0.13 | 0.13 | 0.13 | 0.12 | 0.13 | 0.11 | 0.11 | 0.14 | 0.12 | 0.12 | 0.12 | 0.11 | 0.11 | 0.12 | 0.13 | 0.12 |
| ASI | 3.11 | 1.79 | 1.91 | 2.28 | 1.39 | 1.61 | 2.03 | 1.96 | 1.85 | 2.16 | 2.00 | 2.07 | 2.08 | 1.75 | 2.35 | 1.92 | 1.75 | 2.00 | 1.55 | 2.21 | 1.41 | 1.95 | 1.95 | 2.05 | 2.04 | 2.07 |
| Traces (ppm) | | | | | | | | | | | | | | | | | | | | | | | | | | |
| V | 10 | 61 | 71 | 58 | 80 | 77 | 65 | 72 | 70 | 79 | 77 | 94 | 79 | 76 | 77 | 63 | 66 | 55 | 72 | 75 | 73 | 52 | 63 | 66 | 65 | 65 |
| Cr | 532 | 374 | 534 | 925 | 22 | 1299 | 677 | 903 | 813 | 775 | 1409 | 96 | 575 | 943 | 1326 | 328 | 371 | 467 | 453 | 1803 | 498 | 368 | 276 | 593 | 289 | 1303 |
| Co | 15 | 4.5 | 5.8 | 8.5 | 5 | 7.7 | 8.5 | 8.7 | 9.2 | 9.3 | 9.8 | 15 | 12 | 8.4 | 5.3 | 4.5 | 4.9 | 5.9 | 9.3 | 10 | 6 | 5 | 4.5 | 6.7 | 6.3 | 3.7 |
| Ni | 26 | 22.5 | 28.7 | 36.8 | 27.8 | 31.7 | 20.4 | 22.3 | 15.3 | 27.8 | 22.5 | 68.6 | 38.5 | 25.2 | 25.3 | 31.1 | 27.8 | 32.5 | 50.4 | 179.4 | 26 | 30.7 | 32 | 36.4 | 49 | 23.7 |
| Cu | 2.5 | 1.8 | 1.7 | 3.1 | 1.5 | 1.7 | 2.4 | 2.7 | 2.7 | 1.9 | 2.5 | 2 | 1.3 | 2.3 | 4.1 | 3.6 | 1.3 | 4.5 | 1 | 8 | 2 | 2.7 | 2.9 | 1.2 | 1.2 | 2.7 |
| Zn | 24.9 | 12.2 | 12.8 | 44.8 | 5.1 | 12.8 | 103.7 | 92.5 | 131.8 | 188.2 | 205.2 | 344.3 | 240.7 | 47.7 | 26 | 4.4 | 1.3 | 2.8 | 10.7 | 0.5 | 10.3 | 9.2 | 6 | 1.1 | 0.9 | 0.7 |
| Ga | 43.8 | 39.8 | 41.2 | 60.4 | 34 | 28 | 46.9 | 48.4 | 46.3 | 42.6 | 45.1 | 44.5 | 18.3 | 45.9 | 42.4 | 35 | 36 | 30.7 | 36.2 | 26.1 | 29.7 | 45.8 | 42.4 | 12 | 11.6 | 31.3 |
| As | 9129 | 3.5 | 1.2 | 0.4 | 2.1 | 1 | 38.3 | 41.2 | 0.5 | 1.4 | 1.2 | 27.3 | 8.3 | 5.1 | 0.8 | 4.3 | 6.7 | 2 | 16.1 | 2.5 | 4.3 | 2.9 | 3.2 | 3.4 | 3.8 | 4.1 |
| Rb | 927 | 32 | 571 | 3465 | 487 | 314 | 33 | 20 | 33 | 20 | 21 | 705 | 208 | 85 | 2254 | 38 | 10 | 72 | 975 | 204 | 463 | 352 | 123 | 3 | 3 | 5 |
| Sr | 204.7 | 5.3 | 12.3 | 38.4 | 87.5 | 71.5 | 6.6 | 7.2 | 7.2 | 11.6 | 11 | 13.8 | 4.3 | 15.9 | 21.8 | 113.8 | 150.8 | 36.7 | 87.5 | 55.3 | 73.2 | 9.3 | 1.2 | 137.8 | 141.5 | 226.7 |
| Y | 1.8 | 0.5 | 1.1 | 3 | 1.4 | 0.9 | 0.5 | 0.5 | 0.5 | 0.5 | 0.4 | 1.3 | 0.8 | 0.6 | 2.3 | 0.5 | 0.5 | 0.5 | 1.6 | 0.8 | 1.1 | 0.9 | 0.6 | 0.4 | 0.4 | 0.4 |
| Zr | 251 | 22.7 | 11.7 | 10 | 7.1 | 6.7 | 16.7 | 15.8 | 6.1 | 12 | 9.6 | 46.1 | 4.1 | 32 | 17.9 | 7.7 | 8.7 | 33.8 | 7.6 | 5.9 | 55.2 | 33.8 | 38.8 | 23.1 | 8 | 23.7 |
| Nb | 15 | 73.9 | 19.5 | 29.1 | 3.8 | 9.9 | 45.1 | 59.5 | 74.1 | 27.5 | 57.7 | 54.5 | 2.8 | 35 | 70.5 | 21 | 27.7 | 81.8 | 4.3 | 3.5 | 85.6 | 128.1 | 106 | 4.1 | 3.2 | 20.3 |
| Mo | 8.1 | 2.4 | 3.8 | 3.3 | 2.8 | 3.1 | 2.3 | 5.2 | 2.8 | 2.5 | 2.6 | 6.2 | 5.9 | 2.9 | 3 | 2.4 | 4.3 | 2.6 | 8.4 | 22 | 7.1 | 3.2 | 3.6 | 3.2 | 7.3 | 2.6 |
| Sb | 2.9 | 1.9 | 1.7 | 2.1 | 1.7 | 5.5 | 1.8 | 1.8 | 1.8 | 1.7 | 1.9 | 1.9 | 1.5 | 1.7 | 1.7 | 1.6 | 1.7 | 1.8 | 1.7 | 1.6 | 1.7 | 1.5 | 1.8 | 2 | 1.9 | 1.8 |
| I | 23 | 7.7 | 5.8 | 8 | 5.3 | 5.5 | 7 | 6.5 | 6.4 | 5.7 | 5.8 | 9.9 | 5.4 | 7.1 | 7.2 | 5.3 | 5.1 | 5.7 | 6.1 | 5.5 | 5.6 | 5.7 | 5.8 | 5.8 | 5.4 | 5.1 |
| Cs | 235 | 217 | 115 | 551 | 71 | 32 | 145 | 70 | 29 | 94 | 54 | 74 | 25 | 185 | 244 | 9 | 23 | 9 | 26 | 34 | 37 | 21 | 24 | 9 | 9 | 9 |
| Ba | 501 | 13 | 26 | 14 | 177 | 128 | 69 | 74 | 14 | 211 | 171 | 14 | 13 | 38 | 50 | 149 | 54 | 356 | 494 | 98 | 183 | 19 | 13 | 440 | 490 | 170 |
| La | 20 | 17 | 18 | 19 | 19 | 18 | 19 | 18 | 19 | 19 | 19 | 19 | 22.1 | 18 | 18 | 18 | 18 | 18 | 19 | 18 | 19 | 18 | 18 | 19 | 18.5 | 18 |
| Ce | 31 | 27 | 24 | 28 | 50 | 24 | 33 | 24 | 29 | 25 | 25 | 25 | 24 | 27 | 24 | 29 | 24 | 24 | 25 | 25 | 43 | 48 | 24 | 33 | 35 | 24 |
| Hf | 11.6 | 2.8 | 2.9 | 7.5 | 3.2 | 3.1 | 4.7 | 2.5 | 3.1 | 2.4 | 3 | 3.9 | 3.3 | 3.9 | 7.4 | 3 | 3 | 7.1 | 3.8 | 3.5 | 5 | 2.6 | 4.5 | 3 | 2.9 | 7.3 |
| Ta | 12.4 | 20.1 | 14.7 | 63.7 | 2.9 | 12.7 | 46.4 | 71.7 | 65.6 | 20.5 | 55 | 20.4 | 2.8 | 39.3 | 52.9 | 8.6 | 2.8 | 17.6 | 3.4 | 4.3 | 19.1 | 65.5 | 84.5 | 3 | 3 | 67.3 |
| Pb | 1.5 | 1 | 1.3 | 2.4 | 13.2 | 3.2 | 0.9 | 1 | 0.9 | 0.9 | 0.9 | 1.3 | 1.1 | 1 | 1.9 | 1 | 1 | 1 | 16.9 | 1.7 | 10.2 | 3.7 | 2.7 | 1.9 | 2.9 | 5.4 |
| Bi | 9.8 | 0.9 | 3.4 | 1.6 | 1 | 1 | 1.2 | 1.2 | 1 | 0.9 | 1.1 | 1.2 | 0.9 | 1 | 1.8 | 0.8 | 0.9 | 0.9 | 1.1 | 0.9 | 1 | 1.1 | 1.1 | 0.8 | 0.9 | 58.2 |
| Th | 1.7 | 0.6 | 1.2 | 2.5 | 1.3 | 1 | 0.6 | 0.6 | 0.6 | 0.6 | 0.6 | 0.7 | 0.5 | 0.6 | 2 | 0.7 | 0.7 | 0.6 | 1.4 | 1 | 1 | 0.9 | 0.8 | 0.7 | 0.7 | 1.1 |
| U | 9.7 | 5.7 | 5.9 | 7.9 | 6.4 | 6.6 | 8.4 | 7.2 | 7.7 | 6.6 | 5.4 | 7.6 | 6.5 | 6.9 | 7.2 | 7.1 | 4.7 | 7.1 | 6.9 | 6.2 | 5.8 | 9.4 | 31 | 11 | 6.4 | 5.3 |
| Zr/Hf | 21.64 | 8.11 | 4.03 | 1.33 | 2.22 | 2.16 | 3.55 | 6.32 | 1.97 | 5.00 | 3.20 | 11.82 | 1.24 | 8.21 | 2.42 | 2.57 | 2.90 | 4.76 | 2.00 | 1.69 | 11.04 | 13.00 | 8.62 | 7.70 | 2.76 | 3.25 |
| Nb/Ta | 1.21 | 3.68 | 1.33 | 0.46 | 1.31 | 0.78 | 0.97 | 0.83 | 1.13 | 1.34 | 1.05 | 2.67 | 1.00 | 0.89 | 1.33 | 2.44 | 9.89 | 4.65 | 1.26 | 0.81 | 4.48 | 1.96 | 1.25 | 1.37 | 1.07 | 0.30 |
| Rb/Cs | 3.95 | 0.15 | 4.94 | 6.29 | 6.89 | 9.86 | 0.23 | 0.29 | 1.13 | 0.22 | 0.38 | 9.54 | 8.46 | 0.46 | 9.25 | 4.26 | 0.43 | 7.72 | 37.49 | 5.97 | 12.69 | 16.82 | 5.17 | 0.30 | 0.38 | 0.56 |

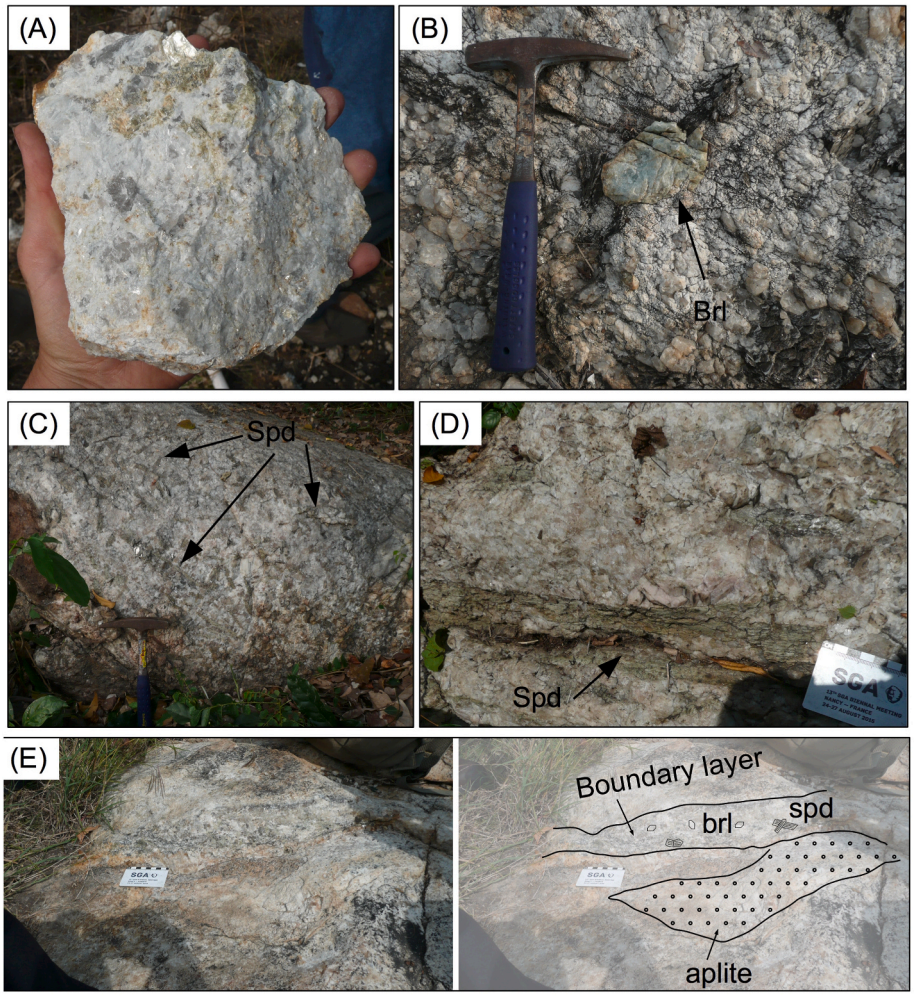


**Fig. 3.** Photographs of the hand samples and outcrops at Mankoadze (A) and Winneba (B–E). (A) Mineralized cleavelanditic albite with greenish mica (MKW6). (B) Coarse-grained blue beryl (WTF1). (C) Disseminated coarse-grained spodumene in quartz-K-feldspar assemblage (WTF3). (D) Giant meter-scale green spodumene (WTF3). (E) Boundary layer enriched in spodumene and beryl at Winneba (WTF4). Spd = spodumene; Brl = beryl.

track the NE-SW Birimian trend, mafic and ultramafic tectonic dykes of the syn- and late-stage also frequently intrude into the rocks. The dykes are around 30 m wide on average, and they partially or completely grade into amphibolite facies (hornblendite). West of Mankoadze, the seashore is covered by metabasalts, which are a sign of late-stage volcanic activity (Nyame, et al., 2021).

## 3. Materials and methods

Ten outcrops were visited in the Mankoadze area and eight in the Winneba area. Their GPS coordinates are given in Table 1. In total, thirty-seven pegmatite samples were collected (twenty from Mankoadze and seventeen from Winneba), and thirty-one were mounted in thin sections. In Table 1, the outcrop names are given in the first column, whereas the sample names are found in the fourth column. Most samples were studied for petrography, mineral assemblages, and mineral geochemistry (Table 1). In addition, twenty-seven of these samples were prepared for whole-rock analyses. The weathered and oxidized parts of the samples were discarded, and the geochemical analysis was performed by X-ray Fluorescence Spectroscopy (XRF) at the Geological Survey Authority of Ghana, Accra, and Instrumental Neutron Activation Analysis (INAA) using the GHARR-1 facility at the Ghana Atomic Energy Commission (GAEC), Kwabenya - Accra, using standard methods.

Polished thin sections were studied under transmitted and reflected light microscopy at the Géosciences Environnement Toulouse (GET) laboratory of the University of Toulouse, France, to determine the mineralogical associations and paragenesis. Backscattered electron (BSE) images were taken with a JEOL scanning electron microscope (SEM) at the GET laboratory, and electron probe microanalyses (EPMA) were performed using a Cameca SX-Five electron microprobe at the Raimond Castaing Centre of the University of Toulouse. The microprobe was operated at 15 kV and 20 nA (except for micas: 10 nA), with a 1 μm focused electron beam (except for micas: 2 μm beam diameter) and a counting time of 10 s for all elements. The following standards were used. For silicates: Topaz (F), $Al_2O_3$ (Al), Wollastonite (Si, Ca), Sanidine (K), Tugtupite (Cl), $MnTiO_3$ (Mn, Ti), $Fe_2O_3$ (Fe), Albite (Na), MgO (Mg), BaSO4 (Ba), Cr2O3 (Cr), Rb, and Cs Glasses. For rare-metal minerals: $LiNbO_3$ (Nb *L*α), metallic W (W Lα), $SnO_2$ (Sn Lα), $TiO_2$ (Ti Kα), $LiTaO_3$ (Ta Lα), $ThO_2$ (Th Mα), $UO_2$ (U Mβ), $ZrSiO_4$ (Zr Lβ), fayalite (Fe Kα), $ScPO_4$ (Sc Kα), Sb (Sb Lα), rhodonite (Mn Kα), MgO (Mg Kα), $YPO_4$ (Y Lα), PbS (Pb Mα), wollastonite (Ca Kα), ZnS (Zn Kα). The data were reduced using the PAP routine (Pouchou and Pichoir, 1985).

## 4. Results

### 4.1. Field relations

The Winneba and Mankoadze pegmatites outcrop in a bushy area along the coastline, about 60 km west of Accra. At Winneba, the outcrops occur as plurimetric boulders along the stream north of Muni

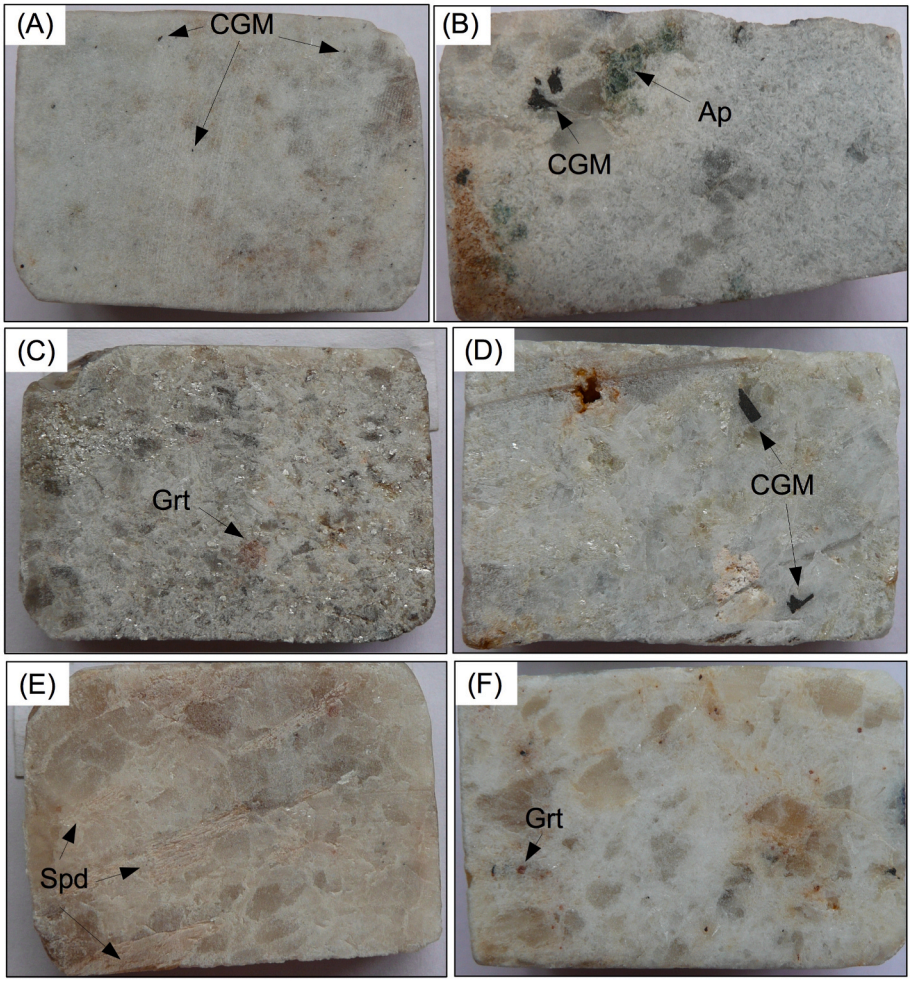


**Fig. 4.** Photographs of the thin section blocks. All blocks are the size of a standard thin section. (A) CGM-rich (all the small black crystals) fine-grained aplite (MKW2A). (B) Coarse-grained apatite and CGM in albitic pegmatite (MKW4). (C) Muscovite-rich greisenised pegmatite with light-red garnet (MTF2). (D) Coarse-grained CGM in muscovite-rich pegmatite (MKW6). (E) Coarse-grained pink spodumene intergrown with quartz and K-feldspar (WTF5). (F) Garnet-rich albitized pegmatite (WIN2B). Ap = apatite; Spd = spodumene; Grt = garnet; CGM = columbite-group minerals.

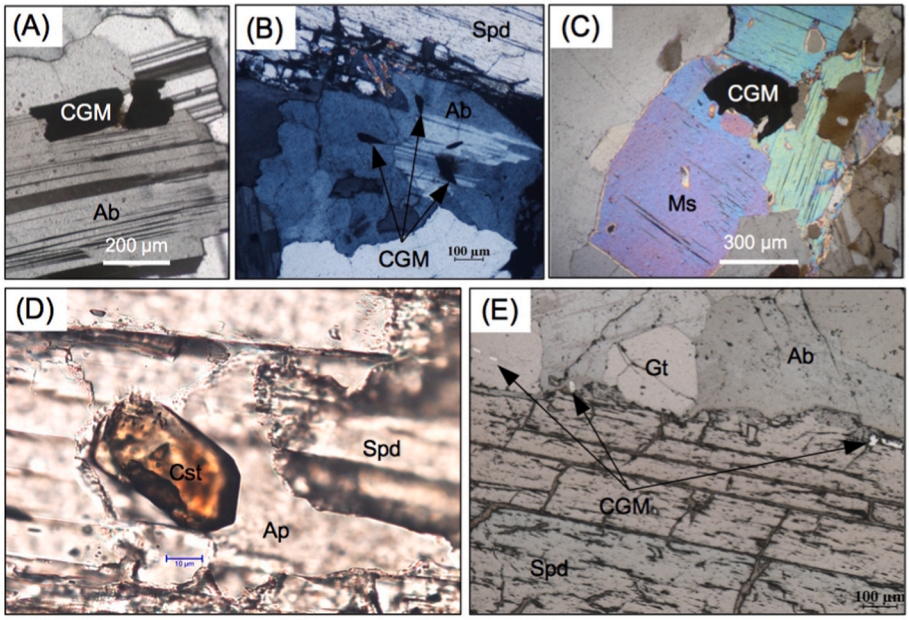


**Fig. 5.** Photomicrographs of Nb–Ta–Sn oxides under optical microscopy. (A–C) CGM intergrown with albite in polarized light (WIN2A and WIN4C). (B) CGM intergrown with muscovite in polarized light (MKW1B). (D) Cassiterite associated with apatite and spodumene in natural light (WIN4C). (E) CGM included in garnet and intergrown with spodumene, evidence of primary magmatic origin (WTF5).

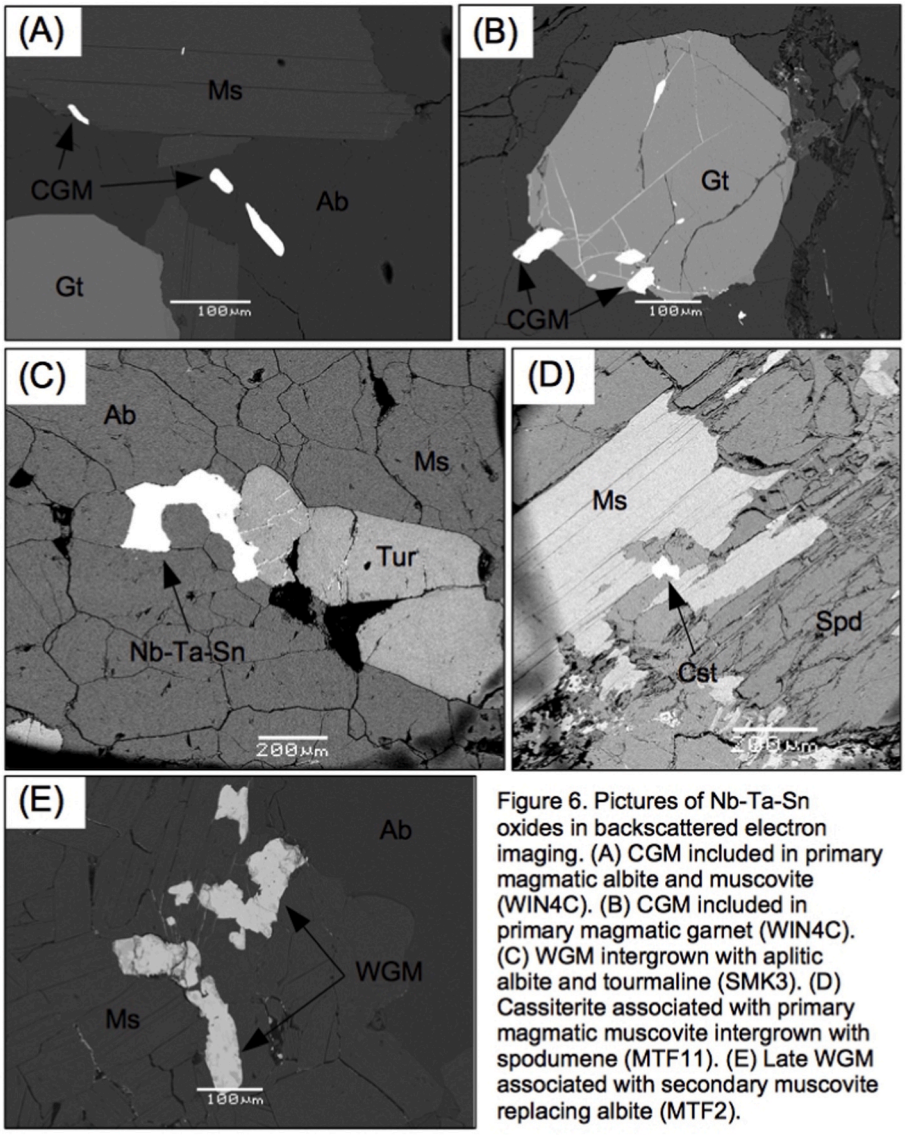


**Fig. 6.** Pictures of Nb–Ta–Sn oxides in backscattered electron imaging. (A) CGM included in primary magmatic albite and muscovite (WIN4C). (B) CGM included in primary magmatic garnet (WIN4C). (C) WGM intergrown with aplitic albite and tourmaline (SMK3). (D) Cassiterite associated with primary magmatic muscovite intergrown with spodumene (MTF11). (E) Late WGM associated with secondary muscovite replacing albite (MTF2).

Lagoon and the Pratu River. They generally form large, tabular isolated outcrops, located between the Muni Lagoon, the Pratu River and the Winneba Senior High School (Fig. 2). One of these pegmatite dykes has a length of up to 30 m in an approximately N–S direction. They are fresh, but their contact with the host rocks are lost, probably because of stream erosion.

In the Mankoadze area, the pegmatites best outcrop on the slopes of the Egyasimanku Hills. The outcrops are generally small (<2 m in length and width) except for one pegmatite outcrop north of Egyasimaku Hills, which is up to 30 m long and 5 m high. According to the lithological map, the pegmatites intrude amphibolites, granodiorites, and quartz-schists, but these country rocks can rarely be observed in the field. The amphibolite, although deeply altered, is observed in trenches dug for mineral exploration at outcrops MKW6 and MKW7. The dykes are generally slightly to moderately weathered. Sulphur-rich veins were also observed in the field intruding the metamafic rocks. In the Mankoadze area, arsenopyrite was observed north of the Mankaamfa Lagoon (Chalokwu et al., 1997). The Winneba granite outcrops about 20 km further to the north and does not appear on Fig. 2.

### 4.2. Pegmatite whole-rock geochemistry

Whole-rock geochemistry of pegmatite rock is not commonly used as a reliable tool to describe pegmatites, as they are by essence too coarse-grained and heterogeneous to get a sample representative of the whole pegmatite body. However, whole-rock geochemistry can give preliminary insights into rare-metal content and degrees of fractionation, provided that they are completed on relatively homogeneous samples without large crystals. To avoid over-interpretation of our whole rock pegmatite results, we completed several analyses for the same outcrop. Results of the whole-rock analyses are shown in Table 2. Relevant rare-metal contents include $P_2O_5$ (generally below 0.1 wt% at Winneba, 0.3 wt% on average and up to 1.5 wt% at Mankoadze), Rb (3–1300 ppm at Winneba, 20–3460 at Mankoadze), Cs (9–59 ppm at Winneba, 10–550 ppm at Mankoadze), Nb (3–130 ppm at Winneba, 3–74 ppm at Mankoadze), and Ta (3–85 ppm at Winneba, 3–72 ppm at Mankoadze). At Mankoadze, the As content is very high, up to 9130 ppm, attesting to the presence of sulfides, which is common in pegmatites intruded in metamafic rocks (Van Lichtervelde et al., 2006). All samples are strongly peraluminous although lithium was not analyzed and would certainly

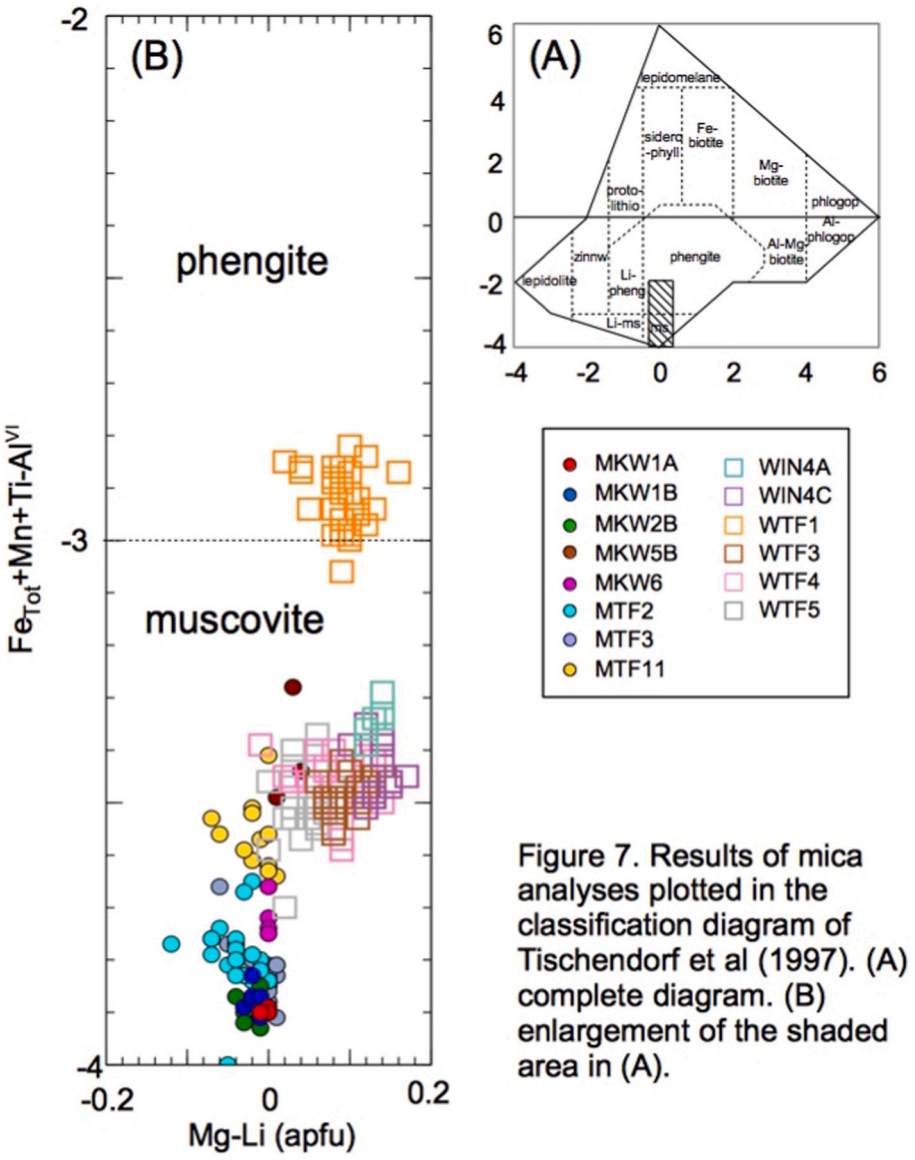


Figure 7. Results of mica analyses plotted in the classification diagram of Tischendorf et al (1997). (A) complete diagram. (B) enlargement of the shaded area in (A).

**Fig. 7.** Results of mica analyses plotted in the classification diagram of Tischendorf et al. (1997). (A) complete diagram. (B) enlargement of the shaded area in (A).

lower the ASI ratios.

### 4.3. Pegmatite mineralogy

The Winneba and Mankoadze pegmatites essentially comprise quartz, K-feldspar, albite, and muscovite. No biotite is observed. The muscovite is yellow-green and may be fine to coarse-grained (Fig. 3A). The Winneba pegmatites are Li-rich and contain mega-crystals of blue beryl (Fig. 3B) and pink or green spodumene (Fig. 3C), which may attain a meter in length (Fig. 3D). Minor red garnet and black tourmaline are common.

Internal zonation inside the pegmatite bodies was not observed except for one outcrop at Winneba (Fig. 3E), where zoning parallel to the pegmatite dyke occurs. The zoning is interpreted as a boundary layer containing large crystals of beryl and spodumene, coexisting with a fine-grained albite layer. The Mankoadze pegmatites host large aplitic units, with some outcrops composed of aplite only (Fig. 4A). The pegmatites in this area are generally albite-rich, with fine-grained green apatite (Fig. 4B), pink garnet (Fig. 4C), turquoise-blue beryl, rare spodumene, and coarse-grained tourmaline which is more common compared to the Winneba pegmatites. The albite occurs as easily recognizable cleavelandite with a bladed morphology and a shiny luster in hand samples (Fig. 3A). The pegmatites can be affected by quartz-muscovite veining or greisen replacement made of fine-grained silvery muscovite (Fig. 4C).

Nb–Ta–Sn mineralization is widespread in all outcrops (Fig. 4A-B-D). It consists of columbite-group minerals (CGM; $[Fe,Mn][Nb,Ta]_2O_6$), wodginite-group minerals (WGM; $[(Mn,Fe)(Sn,Ti,Ta)_2O_8]$) and cassiterite ($SnO_2$), with rarer microlite (the Ta-rich pyrochlore $[(Na,Ca)_2Ta_2O_6(OH,F)]$) and rutile. The crystals are very variable in size, from a few microns to a few millimeters (Fig. 4D). The largest CGM crystal occurs at MKW4 (almost a centimeter in size).

### 4.4. Mineral paragenesis

The accessory silicates (garnet, tourmaline, beryl, and spodumene) are intergrown with the major primary magmatic minerals (quartz, feldspars, and muscovite) and are interpreted as primary magmatic as well (e.g., Fig. 4E). In the aplitic rocks, the minerals are also euhedral and intergrown with no evidence of albite replacement after K-feldspar. However, the cleavelanditic albite commonly replaces earlier pegmatite minerals (Fig. 4F), and it can be interpreted as secondary albitization.

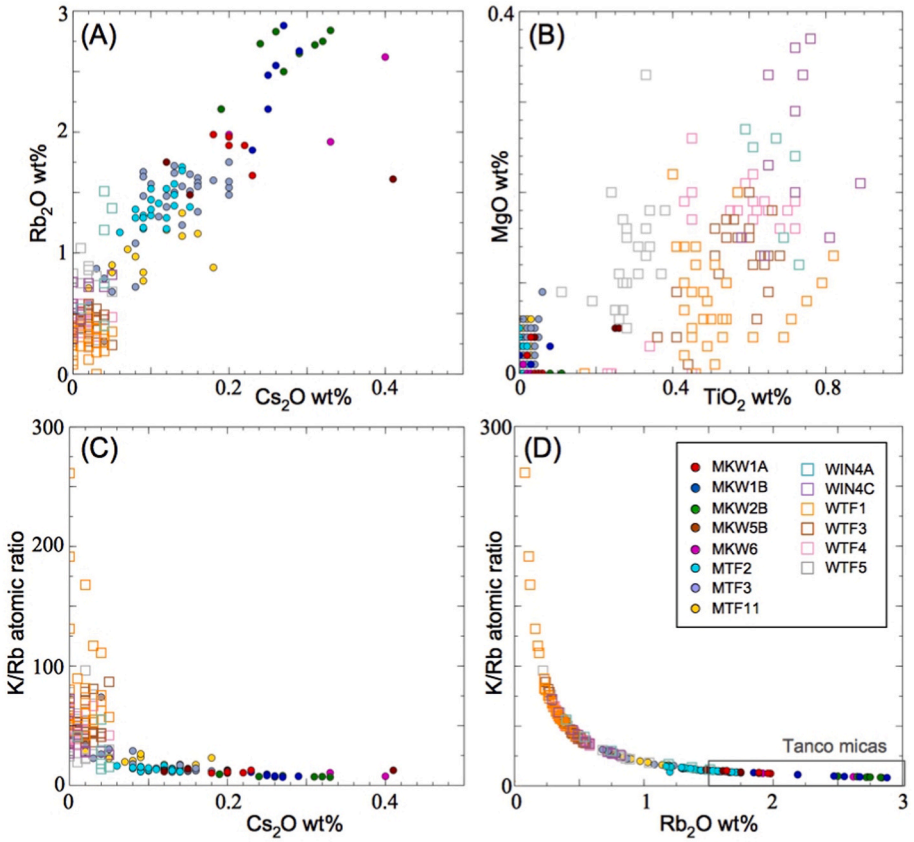


**Fig. 8.** Compositional ranges for micas. (A) Rb versus Cs positive correlation.(B) Mg versus Ti. (C) K/Rb versus Cs. (D) K–Rb Rayleigh fractionation and comparison with the fractionation degree of Tanco pegmatite micas.

Apatite is ubiquitous, i.e., it can occur as early primary rounded crystals intergrown with the primary silicates (Fig. 4B) or as late inter-grain filling.

Both primary and secondary micas were studied. Primary micas are the most abundant and occur extensively in the Winneba area as medium-to coarse-grained euhedral crystals intergrown with or included in spodumene and albite. Secondary micas mostly occur at Mankoadze as greisen-type fine-grained muscovite replacing feldspar (Fig. 4D).

The Nb–Ta–Sn oxides occur as tabular and blocky crystals, euhedral to subhedral in shape (Figs. 5 and 6). They are included in or intergrown with primary rock-forming minerals such as albite, muscovite, garnet, tourmaline, and spodumene. Greisen-type muscovite may host later generations of Nb–Ta–Sn oxides like WGM and microlite (Fig. 6E). Microlite is commonly observed as a replacement of CGM. This reflects hydrothermal or magmatic-metasomatic replacement in CGM, which leads to the development of secondary phases rich in mobile elements such as Fe–Mn–Ca–Ti. Other metamict minerals, interpreted as primary and late secondary, include uranium- and thorium-bearing minerals in the Winneba pegmatite field. With the exception of the Ta–U-rich phase, these metamict minerals will not be further described in this study.

### 4.5. Mineral chemistry

#### 4.5.1. Micas

Mica Electron Probe Microanalyses (EPMA) with their structural formulae are shown in Table 2. They can be classified as pure muscovite, except for one sample from Winneba, WTF1, which plots in the phengite compositional field (Fig. 7). Fluorine is below 0.6 wt%, and lithium is considered to be very low (<0.2 wt% $Li_2O$) based on the Li–F correlation usually observed in pegmatite micas (Roda Robles et al., 2006; Van Lichtervelde et al., 2008). Rubidium and Cs concentrations (<3 wt% $Rb_2O$ and 0.4 wt% $Cs_2O$, Fig. 8A) are considered as normal values for LCT-type pegmatites (Van Lichtervelde et al., 2008). Other minor elements include FeO (<3 wt%), MgO (<0.9 wt%), $TiO_2$ (<0.4 wt%), MnO (<0.2 wt%) and $Na_2O$ (<0.7 wt%). The Mg versus Ti diagram allows the discrimination of the two pegmatite fields (Fig. 8B). Fractionation trends are represented as K/Rb versus Rb and Cs (Fig. 8C–D) and show progressive K–Rb and Rb–Cs fractionation from Winneba to Mankoadze samples.

#### 4.5.2. Garnet

Electron probe microanalyses of garnet are shown in Table 3. The inferred type of garnet is Fe-rich spessartine, with MnO up to 37 wt% (Fig. 9A) and FeO up to 27 wt%. CaO is systematically below 1 wt%. MgO is below 0.2 wt% at Mankoadze, but it is generally above 0.2 wt% at Winneba, with one sample reaching 1.3 wt% (Fig. 9B).

#### 4.5.3. Nb–Ta–Sn oxides

Columbite-group minerals are present in almost all samples, and where absent, WGM are the rare-metal-bearing oxides (Table 1). The average compositions of the CGM and WGM are shown in Tables 4 and 5 and supplementary table 1, respectively. In the columbite quadrilateral Ta/(Ta + Nb) versus Mn/(Mn + Fe), columbite-group minerals occupy the whole compositional field from columbite-Fe to tantalite-Mn and also tapiolite [$FeTa_2O_6$] (Fig. 10). The Winneba and Mankoadze compositions overlap, but the CGM are slightly more fractionated at Mankoadze. Minor elements in the CGM include $TiO_2$ (<2.5 wt%), $SnO_2$ (<1.8 wt%), $UO_2$ (<1.2 wt%), $WO_3$ (<0.8 wt%), $ZrO_2$ (<0.6 wt%), and $Sc_2O_3$ (<0.14 wt%). The Ti versus Sn plot reveals very distinct compositional fields between the Winneba and Mankoadze samples (Fig. 11).

Wodginite-group minerals (WGM) are not common at Winneba, but

**Table 3**
Mica EPMA analyses (average composition in wt.% and standard deviation on N analyses) and structural formulae calculated on 24 (O, OH, F).

| | WIN4A | *N = 6* | WIN4C | *N = 11* | WTF1 | *N = 31* | WTF3 | *N = 24* | WTF4 | *N = 24* | WTF5 | *N = 25* | MKW1A | *N = 5* | MKW1B | *N = 6* | MKW2B | *N = 8* | MKW5B | *N = 3* | MKW6 | *N = 4* | MTF2 | *N = 23* | MTF3 | *N = 31* | MTF11 | *N = 12* |
|---|---|---|---|---|---|---|---|---|---|---|---|---|---|---|---|---|---|---|---|---|---|---|---|---|---|---|---|---|
| SiO2 | 44.62 | *0.15* | 44.82 | *0.35* | 44.20 | *0.35* | 44.51 | *0.31* | 44.44 | *0.31* | 43.96 | *0.35* | 44.50 | *0.10* | 44.19 | *0.53* | 44.27 | *0.17* | 44.86 | *0.35* | 44.49 | *0.28* | 44.14 | *0.56* | 44.28 | *0.46* | 43.99 | *0.63* |
| TiO2 | 0.21 | *0.06* | 0.25 | *0.09* | 0.08 | *0.05* | 0.12 | *0.05* | 0.16 | *0.07* | 0.12 | *0.06* | 0.01 | *0.02* | 0.02 | *0.02* | 0.00 | *0.00* | 0.04 | *0.00* | 0.00 | *0.01* | 0.02 | *0.01* | 0.03 | *0.02* | 0.04 | *0.01* |
| Al2O3 | 34.13 | *0.28* | 34.08 | *0.42* | 31.56 | *0.38* | 33.89 | *0.28* | 33.78 | *0.41* | 34.49 | *0.38* | 36.44 | *0.22* | 36.35 | *0.33* | 36.49 | *0.36* | 34.05 | *0.70* | 35.74 | *0.30* | 35.87 | *0.64* | 36.23 | *0.40* | 34.48 | *0.49* |
| FeO | 2.44 | *0.12* | 1.95 | *0.09* | 4.55 | *0.22* | 1.78 | *0.12* | 1.87 | *0.23* | 2.00 | *0.19* | 0.28 | *0.03* | 0.30 | *0.05* | 0.18 | *0.04* | 2.50 | *0.32* | 1.28 | *0.17* | 0.83 | *0.16* | 0.86 | *0.09* | 1.85 | *0.25* |
| MnO | 0.06 | *0.03* | 0.07 | *0.04* | 0.07 | *0.01* | 0.12 | *0.04* | 0.10 | *0.03* | 0.10 | *0.03* | 0.06 | *0.03* | 0.04 | *0.02* | 0.05 | *0.04* | 0.07 | *0.05* | 0.02 | *0.01* | 0.08 | *0.05* | 0.05 | *0.04* | 0.11 | *0.06* |
| MgO | 0.67 | *0.06* | 0.71 | *0.09* | 0.52 | *0.13* | 0.56 | *0.09* | 0.54 | *0.14* | 0.29 | *0.07* | 0.04 | *0.02* | 0.04 | *0.03* | 0.07 | *0.03* | 0.18 | *0.12* | 0.02 | *0.01* | 0.01 | *0.01* | 0.03 | *0.02* | 0.02 | *0.02* |
| CaO | 0.00 | *0.01* | 0.01 | *0.01* | 0.01 | *0.02* | 0.01 | *0.01* | 0.01 | *0.02* | 0.01 | *0.01* | 0.01 | *0.02* | 0.03 | *0.02* | 0.01 | *0.02* | 0.02 | *0.03* | 0.02 | *0.02* | 0.01 | *0.02* | 0.01 | *0.02* | 0.01 | *0.02* |
| Li2O (c) | 0.01 | *0.00* | 0.02 | *0.03* | 0.02 | *0.03* | 0.02 | *0.03* | 0.04 | *0.05* | 0.02 | *0.03* | 0.02 | *0.00* | 0.05 | *0.01* | 0.07 | *0.01* | 0.03 | *0.01* | 0.01 | *0.00* | 0.07 | *0.03* | 0.02 | *0.02* | 0.03 | *0.03* |
| Na2O | 0.32 | *0.04* | 0.27 | *0.03* | 0.42 | *0.09* | 0.48 | *0.12* | 0.50 | *0.12* | 0.40 | *0.09* | 0.36 | *0.03* | 0.36 | *0.02* | 0.30 | *0.04* | 0.38 | *0.16* | 0.37 | *0.09* | 0.31 | *0.05* | 0.33 | *0.06* | 0.28 | *0.09* |
| K2O | 10.87 | *0.30* | 10.39 | *0.14* | 10.17 | *0.29* | 10.12 | *0.28* | 10.13 | *0.23* | 10.33 | *0.25* | 10.37 | *0.19* | 10.15 | *0.12* | 10.10 | *0.20* | 10.18 | *0.05* | 10.18 | *0.09* | 9.65 | *0.61* | 9.80 | *0.32* | 10.12 | *0.14* |
| F | 0.06 | *0.03* | 0.10 | *0.15* | 0.14 | *0.18* | 0.15 | *0.15* | 0.16 | *0.19* | 0.13 | *0.15* | 0.15 | *0.03* | 0.24 | *0.06* | 0.32 | *0.07* | 0.16 | *0.10* | 0.05 | *0.02* | 0.33 | *0.17* | 0.14 | *0.14* | 0.17 | *0.18* |
| Rb2O | 0.96 | *0.46* | 0.59 | *0.18* | 0.29 | *0.11* | 0.43 | *0.09* | 0.45 | *0.08* | 0.52 | *0.24* | 1.87 | *0.14* | 2.43 | *0.37* | 2.65 | *0.22* | 1.61 | *0.13* | 2.18 | *0.32* | 1.39 | *0.15* | 1.35 | *0.38* | 0.98 | *0.19* |
| Cs2O | 0.04 | *0.01* | 0.01 | *0.02* | 0.02 | *0.02* | 0.02 | *0.01* | 0.01 | *0.01* | 0.01 | *0.01* | 0.20 | *0.02* | 0.26 | *0.02* | 0.28 | *0.05* | 0.23 | *0.16* | 0.28 | *0.10* | 0.11 | *0.02* | 0.12 | *0.05* | 0.10 | *0.05* |
| Total | 94.38 | *0.43* | 93.30 | *0.32* | 92.12 | *0.55* | 92.24 | *0.46* | 92.20 | *0.43* | 92.37 | *0.49* | 94.28 | *0.48* | 94.41 | *0.66* | 94.71 | *0.48* | 94.28 | *0.29* | 94.64 | *0.12* | 92.78 | *0.71* | 93.25 | *0.62* | 92.19 | *0.79* |
| Atoms per 24 (O, OH, F) | | | | | | | | | | | | | | | | | | | | | | | | | | | | |
| Si IV | 6.13 | | 6.17 | | 6.23 | | 6.17 | | 6.17 | | 6.11 | | 6.08 | | 6.05 | | 6.05 | | 6.18 | | 6.10 | | 6.08 | | 6.08 | | 6.13 | |
| Al IV | 1.87 | | 1.83 | | 1.77 | | 1.83 | | 1.83 | | 1.89 | | 1.92 | | 1.95 | | 1.95 | | 1.82 | | 1.90 | | 1.92 | | 1.92 | | 1.87 | |
| Sum IV | 8.00 | | 8.00 | | 8.00 | | 8.00 | | 8.00 | | 8.00 | | 8.00 | | 8.00 | | 8.00 | | 8.00 | | 8.00 | | 8.00 | | 8.00 | | 8.00 | |
| Al VI | 3.65 | | 3.70 | | 3.47 | | 3.72 | | 3.70 | | 3.75 | | 3.94 | | 3.92 | | 3.92 | | 3.70 | | 3.87 | | 3.90 | | 3.94 | | 3.80 | |
| Ti | 0.02 | | 0.03 | | 0.01 | | 0.01 | | 0.02 | | 0.01 | | 0.00 | | 0.00 | | 0.00 | | 0.00 | | 0.00 | | 0.00 | | 0.00 | | 0.00 | |
| Fe2+ | 0.28 | | 0.22 | | 0.54 | | 0.21 | | 0.22 | | 0.23 | | 0.03 | | 0.03 | | 0.02 | | 0.29 | | 0.15 | | 0.10 | | 0.10 | | 0.22 | |
| Mn | 0.01 | | 0.01 | | 0.00 | | 0.01 | | 0.01 | | 0.01 | | 0.01 | | 0.00 | | 0.01 | | 0.01 | | 0.00 | | 0.01 | | 0.01 | | 0.01 | |
| Mg | 0.14 | | 0.15 | | 0.11 | | 0.12 | | 0.11 | | 0.06 | | 0.01 | | 0.01 | | 0.01 | | 0.04 | | 0.00 | | 0.00 | | 0.01 | | 0.00 | |
| LiVI | 0.00 | | 0.00 | | 0.02 | | 0.02 | | 0.02 | | 0.01 | | 0.01 | | 0.03 | | 0.04 | | 0.01 | | 0.00 | | 0.04 | | 0.01 | | 0.02 | |
| SumVI | 4.10 | | 4.10 | | 4.14 | | 4.08 | | 4.07 | | 4.08 | | 4.00 | | 3.99 | | 3.99 | | 4.06 | | 4.03 | | 4.05 | | 4.06 | | 4.05 | |
| Na | 0.08 | | 0.07 | | 0.12 | | 0.13 | | 0.13 | | 0.11 | | 0.09 | | 0.10 | | 0.08 | | 0.10 | | 0.10 | | 0.08 | | 0.09 | | 0.08 | |
| K | 1.90 | | 1.82 | | 1.83 | | 1.79 | | 1.80 | | 1.83 | | 1.81 | | 1.77 | | 1.76 | | 1.79 | | 1.78 | | 1.70 | | 1.72 | | 1.80 | |
| Rb | 0.08 | | 0.05 | | 0.03 | | 0.04 | | 0.04 | | 0.05 | | 0.16 | | 0.21 | | 0.23 | | 0.14 | | 0.19 | | 0.12 | | 0.12 | | 0.09 | |
| Cs | 0.00 | | 0.00 | | 0.00 | | 0.00 | | 0.00 | | 0.00 | | 0.01 | | 0.01 | | 0.02 | | 0.01 | | 0.02 | | 0.01 | | 0.01 | | 0.01 | |
| SUM A | 2.07 | | 1.95 | | 1.97 | | 1.96 | | 1.97 | | 1.99 | | 2.08 | | 2.10 | | 2.09 | | 2.05 | | 2.09 | | 1.91 | | 1.93 | | 1.97 | |

Li2O (C) calculated after Roda Robles et al. (2006). H2O is not calculated.

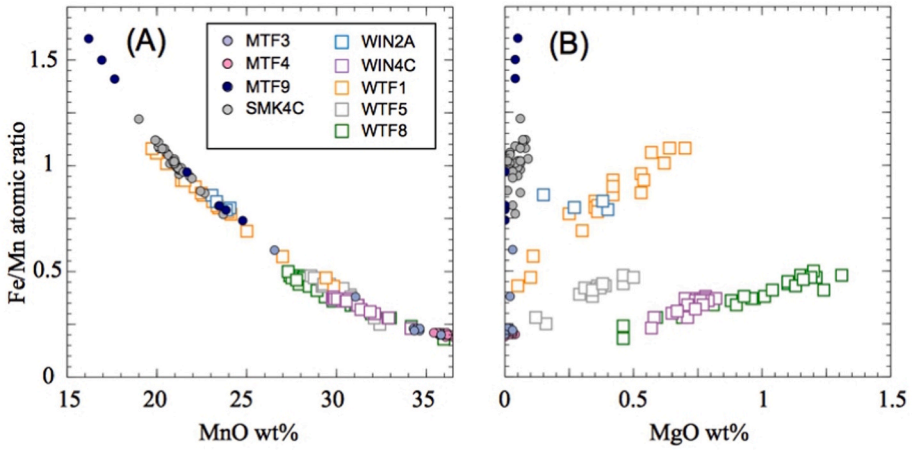


**Fig. 9.** (A) Fe–Mn Rayleigh fractionation diagram and (B) Fe/Mn versus MgO diagrams for garnet.

they are present in almost all samples from Mankoadze. Their compositions are highly variable, thus, 34.7–67.2 wt% $Ta_2O_5$, 3.4–23.5 wt% $Nb_2O_5$, 4.5–17.8 wt% $SnO_2$, 0.1–8.8 wt% $TiO_2$, 1.8–11.3 wt% FeO, 1.2–10.7 wt% MnO, 0.1–2.3 wt% $ZrO_2$, and <1.2 wt% $WO_3$. The low totals may reflect the presence of $Fe_2O_3$ instead of FeO. The only WGM analyzed from the Winneba samples is Ti-wodginite, with an average $TiO_2$ concentration of 7.8 wt%. Some lithiowodginite may also be present, but Li was not analyzed in our samples. In the columbite quadrilateral (Fig. 12), the WGM display Mn/(Mn + Fe) ratios similar to those of the CGM associated in the same samples, but the former is slightly more fractionated in terms of Nb/Ta than the latter.

Cassiterite occasionally occurs at Mankoadze and rarely at Winneba. It may host elevated Ta concentrations (up to 7 wt% $Ta_2O_5$ in MKW4). Other accessory minerals include zircon, pyrochlore, and unidentified metamict U–Th-bearing minerals. One of the metamict minerals reveals an uncommon composition with Ta and U as major elements. Most euhedral crystals have angular orthorhombic or cubic shapes (Fig. 13). It is not pyrochlore because of the absence of Na and Ca in its composition, and it is associated with "true" microlite crystals. The closest known International Mineralogical Association composition is uranopolycrase.

## 5. Discussion

### 5.1. Classification of the pegmatites

The Winneba and Mankoadze pegmatites present all characteristics of pegmatites from the rare-element class and Lithium–Cesium–Tantalum (LCT) family as described by Černý and Ercit (2005). They are granitic and peraluminous in composition, with K-feldspar, albite, quartz, and muscovite (no biotite) as major minerals, and garnet, tourmaline, beryl, apatite, and Nb–Ta–Sn oxides as accessory minerals. The pegmatites at Winneba host very large metric crystals of spodumene, that make up to 20% of the rock volume, whereas at Mankoadze, they are more albite-rich with aplitic textures. Moreover, the Mankoadze pegmatites are phosphorus-rich, with a positive P–Ca correlation in whole-rock that attests to the ubiquitous presence of apatite in this area.

The CGM ranges from columbite-(Fe) to tantalite-(Mn); it is primary magmatic and crystallizes with the silicate minerals feldspars (microcline and albite); spodumene; garnet, and mica. Micas plot in the compositional field of pure muscovite after the classification diagram of Tischendorf et al. (1997) (Fig. 7). The only difference in composition is the phengite found in micas of the sample WTF1, which are embedded in spodumene, evidence of their primary magmatic origin. In the absence of lepidolite or even Li-rich muscovite or phengite, the Winneba-Mankoadze pegmatites cannot be classified as complex type. The absence of major phosphate minerals such as amblygonite is also to be noted.

Garnets in the studied samples have high concentrations of Mn and low concentrations of Ca, similar to garnet concentrations in pegmatites reported worldwide (Baldwin and Von Knorring, 1983; Bekele and Sen, 2020). The type of garnet inferred is Fe-rich spessartine. Spessartine-rich garnet is usually associated with Li-rich pegmatites worldwide and commonly crystallizes at pressures below 5 kbar to less than 1 kbar at 750 °C in granitic pegmatitic magma (Manning, 1983; Bekele and Sen, 2020). Consequently, the studied pegmatites can be classified as the albite-spodumene type after Černý and Ercit (2005).

Finally, zoning in the studied pegmatites is relatively simple, although layering features that could be interpreted as boundary layers are observed (Fig. 3E). These features typically form in supercooled and/or flux-rich liquids where fast crystallization triggers the accumulation of incompatible elements in a melt layer at the crystallization front of the solid rock (London, 2014; London and Morgan, 2017). In Fig. 3E, the incompatible elements Be and Li accumulated in the boundary layer. the presence of aplitic rock is also evidence of local chemical quenching when flux elements (Li, F, B, $H_2O$ etc.) are lost from the melt, which abruptly increases the solidus temperature (London, 1987). All these features argue for a flux-rich (Li, F, B, P, and Be) granitic melt that was emplaced in cold country rocks at a relatively shallow crustal level (3–4 kbars) as the origin of the albite-spodumene pegmatites (Černý, 1991).

### 5.2. Evidence of two distinct pegmatite fields

Field observations suggest that the two pegmatite groups at Winneba and Mankoadze compose distinct fields. The Winneba field extends over 2.4 km in a NNW-SSE direction, whereas the Mankoadze field extends over 5 km in a SW-NE direction (Fig. 2). The two pegmatite fields are separated by a distance of approximately 3 km. However, there could be a sampling bias due to the presence of the lagoon between the two villages, and it is possible that further exploration for mining purposes would reveal continuity between the two fields.

The mineralogy is similar between the two fields, although Mankoadze is more sodic, with widespread albitization and aplite zones. Mankoadze is also more mineralized in Nb–Ta–Sn, whereas the Winneba field is more mineralized in Li, with large spodumene crystals that are not seen in Mankoadze. More generally, the Mankoadze pegmatites seem to be more evolved. In whole-rock, the fractionation degree is different between Winneba and Mankoadze, with the former being poorer in Nb–Ta and Rb–Cs.

Mineral chemistry shows considerable differences between the two fields. Micas are clearly more fractionated at Mankoadze, where the highest values in micas attain 2.6 wt% $Rb_2O$ and 0.4 wt% $Cs_2O$, than at

**Table 4**
EPMA composition (sample average in wt.% and standard deviation on *N* analyses) of garnet.

| | MTF3 | *N = 8* | MTF4 | *N = 26* | MTF9 | *N = 7* | SMK4C | *N = 34* | WIN2A | *N = 4* | WIN4C | *N = 23* | WTF1 | *N = 19* | WTF5 | *N = 13* | WTF8 | *N = 25* |
|---|---|---|---|---|---|---|---|---|---|---|---|---|---|---|---|---|---|---|
| Na2O | 0.01 | *0.01* | 0.01 | *0.01* | 0.00 | *0.01* | 0.02 | *0.02* | 0.01 | *0.01* | 0.01 | *0.01* | 0.02 | *0.01* | 0.02 | *0.02* | 0.04 | *0.03* |
| Al2O3 | 20.35 | *0.15* | 20.73 | *0.11* | 20.23 | *0.08* | 20.12 | *0.12* | 20.12 | *0.13* | 20.60 | *0.12* | 20.05 | *0.22* | 20.61 | *0.09* | 20.14 | *0.27* |
| SiO2 | 36.19 | *0.17* | 36.25 | *0.47* | 36.24 | *0.15* | 36.05 | *0.16* | 35.61 | *0.30* | 36.40 | *0.27* | 36.07 | *0.30* | 36.37 | *0.34* | 36.36 | *0.30* |
| CaO | 0.27 | *0.10* | 0.23 | *0.08* | 0.39 | *0.09* | 0.32 | *0.05* | 0.43 | *0.04* | 0.51 | *0.16* | 0.31 | *0.18* | 0.67 | *0.58* | 0.25 | *0.20* |
| MnO | 33.22 | *3.02* | 35.91 | *0.26* | 20.65 | *3.63* | 21.06 | *0.96* | 23.58 | *0.47* | 30.97 | *1.13* | 23.19 | *2.93* | 30.06 | *1.19* | 29.71 | *2.32* |
| FeO | 9.36 | *3.08* | 7.38 | *0.16* | 22.14 | *3.41* | 21.39 | *0.98* | 19.61 | *0.39* | 10.69 | *0.87* | 19.06 | *2.43* | 12.18 | *1.66* | 11.59 | *1.87* |
| MgO | 0.01 | *0.01* | 0.01 | *0.01* | 0.02 | *0.02* | 0.05 | *0.02* | 0.30 | *0.12* | 0.73 | *0.07* | 0.40 | *0.19* | 0.34 | *0.11* | 0.98 | *0.25* |
| TiO2 | 0.00 | *0.00* | 0.04 | *0.03* | 0.00 | *0.00* | 0.01 | *0.01* | 0.04 | *0.03* | 0.08 | *0.03* | 0.01 | *0.02* | 0.05 | *0.03* | 0.04 | *0.06* |
| Total | 99.40 | *0.48* | 100.58 | *0.47* | 99.69 | *0.22* | 99.01 | *0.29* | 99.73 | *0.44* | 100.00 | *0.41* | 99.12 | *0.31* | 100.32 | *0.51* | 99.12 | *0.46* |

Winneba, where most mica analyses are below 1 wt% $Rb_2O$ and below the detection limit for Cs (Table 2, Fig. 8A). The least fractionated mica, phengite, with FeO average composition of 4.5 wt%, occurs at Winneba and displays the lowest $Rb_2O$ composition (average 0.3 wt%). The Mg versus Ti diagram (Fig. 8B) is also clearly discriminant, with the Winneba micas being ten times richer in Mg and Ti than the Mankoadze micas. For garnet, the two fields are comparable in terms of fractionation degree (Fig. 9A), but they can be clearly distinguished by their Mg content (Fig. 9B). In the CGM, the fractionation degree is higher at Mankoadze than at Winneba (Fig. 10), and the Ti versus Sn plot discriminates between the two areas (Fig. 11). Elevated Ti concentrations are recorded in the WGM of Winneba but not at Mankoadze. These chemical features suggest that melt fractionation is not the only parameter that controls mineral chemistry, and some minor elements such as Ti and Mg could be controlled by different processes.

At Winneba, the Mg content of garnet increases with increasing fractionation, and several trends are observed (Fig. 9B). This is not consistent with a fractionation model (e.g., Hernández-Filiberto et al., 2021), i.e., Mg was not incorporated from the liquid into garnet via simple fractional crystallization, and other processes may have influenced the Mg content. In particular, it is possible that contamination of the liquid occurred from the mafic country rocks, especially the neighbouring metamafic dykes.

### 5.3. Fractionation trends in the pegmatites

The Winneba-Mankoadze pegmatites have whole-rock concentrations that show elevated rare metal contents typical of rare-element granites and pegmatites (Koffi Brou et al., 2022): Cs up to 100 × UCC (UCC = upper continental crust of Rudnick and Gao (2003)), Ta up to 85 × UCC, Nb = 10 × UCC. The Nb/Ta ratio is below 13 and mostly below 5 in both areas, which suggests a strong degree of fractionation (Ballouard et al., 2016). In the rock-forming minerals of granites, some element ratios evolve with fractional crystallization of the melt because these elements substitute for each other in a 1:1 atomic ratio. This is the case of the alkali metals K, Rb, and Cs in mica, Nb and Ta in the CGM, or Fe and Mn in garnet (Černý et al., 1985). Usually, an incompatible element substitutes for a more compatible one with increasing fractionation, and their incorporation in minerals is controlled by their partition coefficients (Černý et al., 1985). For example, in granites, K-feldspar and muscovite precipitation leads to the preferential uptake of K from the melt and subsequent Rb accumulation in the residual liquid; hence, the decrease in K/Rb values in these minerals during granitic melt evolution (Černý et al., 1985). The X/Y versus Y element diagrams are used to compare relative fractionation levels, and these can be used to quantitatively model Rayleigh-type fractionation in granite-pegmatite systems (Hulsbosch et al., 2014).

The Winneba-Mankoadze pegmatites can be compared to other rare-element pegmatites in the world in terms of fractionation degree. At Mankoadze, most micas contain concentrations above 1 wt% $Rb_2O$. This corresponds to K/Rb ratios below 30, which fall in the compositional field of the most fractionated pegmatites (Fig. 8D). For comparison, K/Rb ratios in muscovite from the Austroalpine albite-spodumene rare-element pegmatites are 15–150 (Knoll et al., 2023), those from the Kenticha complex rare-element pegmatite of the spodumene subtype are 7–42 in average (Küster et al., 2009), and those from the complex Tanco pegmatite are below 15 (Van Lichtervelde et al., 2008). Columbite-group minerals are the most common Nb–Ta ores worldwide, and they are commonly used as fractionation indicators in pegmatites. The Nb/Ta ratio of CGM is either controlled by the solubilities of its end-members (Linnen and Keppler, 1997) or by CGM supersaturation in the melt. In the former case, the tantalite end-member is more soluble than the columbite end-member at a given temperature, and early crystallized CGM tends towards the Nb-rich end-member, whereas later CGM tends towards the Ta-rich pole. In the latter case, strong supersaturation (i.e., Nb and Ta contents in the melt well above saturation

**Table 5**
EPMA composition (sample average in wt.% and standard deviation on *N* analyses) of the WGM and structural formulae on 8 oxygens.

| | MKW4A | *N = 10* | MKW5B | *N = 2* | MTF2 | *N = 48* | MTF3 | *N = 24* | MTF6 | *N = 11* | SMK3 | *N = 19* | WIN4C | *N = 4* |
|---|---|---|---|---|---|---|---|---|---|---|---|---|---|---|
| Nb2O5 | 10.07 | *1.06* | 8.94 | *1.20* | 8.69 | *2.50* | 7.81 | *1.08* | 11.11 | *4.84* | 8.16 | *0.48* | 14.72 | *0.75* |
| Ta2O5 | 60.74 | *1.31* | 60.42 | *1.54* | 59.77 | *2.64* | 61.82 | *1.54* | 59.95 | *3.35* | 60.72 | *0.72* | 54.53 | *0.38* |
| MnO | 4.56 | *0.25* | 5.49 | *0.39* | 8.81 | *0.71* | 7.82 | *1.65* | 4.37 | *0.84* | 6.27 | *0.33* | 7.00 | *0.55* |
| FeO | 8.25 | *0.42* | 7.18 | *0.02* | 3.67 | *0.78* | 5.00 | *1.71* | 7.81 | *2.18* | 6.57 | *0.47* | 6.96 | *0.67* |
| ZrO2 | 0.67 | *0.21* | 0.52 | *0.22* | 1.63 | *0.33* | 1.09 | *0.33* | 0.48 | *0.19* | 0.61 | *0.09* | 0.38 | *0.13* |
| SnO2 | 12.81 | *0.93* | 13.05 | *0.48* | 14.57 | *1.38* | 12.77 | *1.22* | 8.88 | *2.33* | 13.65 | *0.67* | 5.99 | *0.19* |
| Sc2O3 | 0.02 | *0.01* | 0.02 | *0.01* | 0.01 | *0.01* | 0.02 | *0.01* | 0.03 | *0.02* | 0.02 | *0.01* | 0.01 | *0.01* |
| WO3 | 0.13 | *0.14* | 0.42 | *0.42* | 0.55 | *0.31* | 0.40 | *0.17* | 0.14 | *0.11* | 0.22 | *0.19* | 0.14 | *0.07* |
| TiO2 | 1.19 | *0.12* | 0.93 | *0.05* | 0.20 | *0.07* | 0.55 | *0.50* | 2.24 | *0.46* | 0.18 | *0.06* | 7.74 | *0.33* |
| PbO | 0.01 | *0.02* | 0.06 | *0.08* | 0.04 | *0.05* | 0.03 | *0.04* | 0.01 | *0.02* | 0.02 | *0.04* | 0.10 | *0.08* |
| ThO2 | 0.00 | *0.00* | 0.00 | *0.00* | 0.05 | *0.07* | 0.05 | *0.08* | 0.03 | *0.05* | 0.04 | *0.06* | 0.04 | *0.07* |
| UO2 | 0.00 | *0.00* | 0.00 | *0.00* | 0.01 | *0.04* | 0.00 | *0.00* | 0.00 | *0.01* | 0.00 | *0.00* | 0.03 | *0.05* |
| Total | 98.51 | *0.80* | 97.03 | *0.25* | 98.00 | *0.55* | 97.34 | *0.36* | 95.03 | *3.21* | 96.46 | *0.54* | 97.63 | *0.69* |
| Atoms per formula unit for 8 O | | | | | | | | | | | | | | |
| Fe | 0.72 | *0.04* | 0.64 | *0.00* | 0.33 | *0.07* | 0.45 | *0.15* | 0.69 | *0.18* | 0.60 | *0.04* | 0.56 | *0.05* |
| Mn | 0.41 | *0.02* | 0.50 | *0.03* | 0.80 | *0.07* | 0.72 | *0.15* | 0.39 | *0.07* | 0.58 | *0.03* | 0.58 | *0.05* |
| Ti | 0.09 | *0.01* | 0.08 | *0.00* | 0.02 | *0.01* | 0.04 | *0.04* | 0.18 | *0.03* | 0.01 | *0.00* | 0.56 | *0.03* |
| Nb | 0.48 | *0.05* | 0.43 | *0.05* | 0.42 | *0.11* | 0.38 | *0.05* | 0.53 | *0.21* | 0.40 | *0.02* | 0.65 | *0.03* |
| Ta | 1.73 | *0.05* | 1.76 | *0.06* | 1.74 | *0.10* | 1.82 | *0.05* | 1.74 | *0.14* | 1.80 | *0.03* | 1.44 | *0.01* |
| Sn | 0.54 | *0.04* | 0.56 | *0.03* | 0.62 | *0.06* | 0.55 | *0.05* | 0.38 | *0.11* | 0.59 | *0.03* | 0.23 | *0.01* |
| W | 0.00 | *0.00* | 0.01 | *0.01* | 0.02 | *0.01* | 0.01 | *0.00* | 0.00 | *0.00* | 0.01 | *0.01* | 0.00 | *0.00* |
| Zr | 0.03 | *0.01* | 0.03 | *0.01* | 0.08 | *0.02* | 0.06 | *0.02* | 0.02 | *0.01* | 0.03 | *0.00* | 0.02 | *0.01* |
| Total | 4.01 | *0.01* | 4.02 | *0.01* | 4.02 | *0.01* | 4.03 | *0.01* | 4.03 | *0.01* | 4.04 | *0.01* | 4.05 | *0.00* |

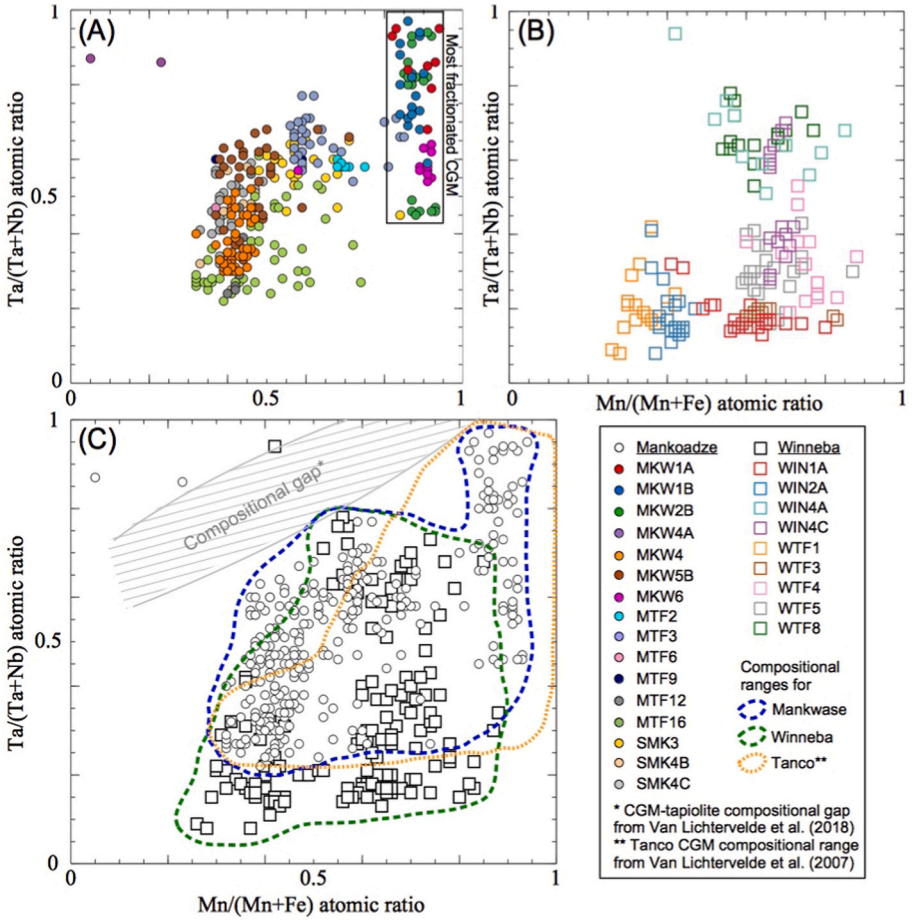


**Fig. 10.** CGM and WGM analyses in the columbite quadrilateral. (A) CGM of Mankoadze, (B) CGM of Winneba (C) comparison of the two fields with the CGM field of a highly differentiated pegmatite, the Tanco pegmatite in Canada.

values for CGM at a given temperature, see Van Lichtervelde et al., 2018) leads to oscillatory zoning with extensive Nb–Ta oscillations between Nb- and Ta-rich poles (Van Lichtervelde et al., 2018). The CGM compositions in the Winneba-Mankoadze pegmatites reveal extreme Nb/Ta fractionation, typical of highly fractionated complex spodumene, petalite, or lepidolite-type pegmatites enriched in fluorine and lithium (Černý, 1989; Černý and Ercit, 1989; Tindle and Breaks, 2000; Llorens and Moro, 2012; Bekele and Sen, 2020). Garnet shows extensive

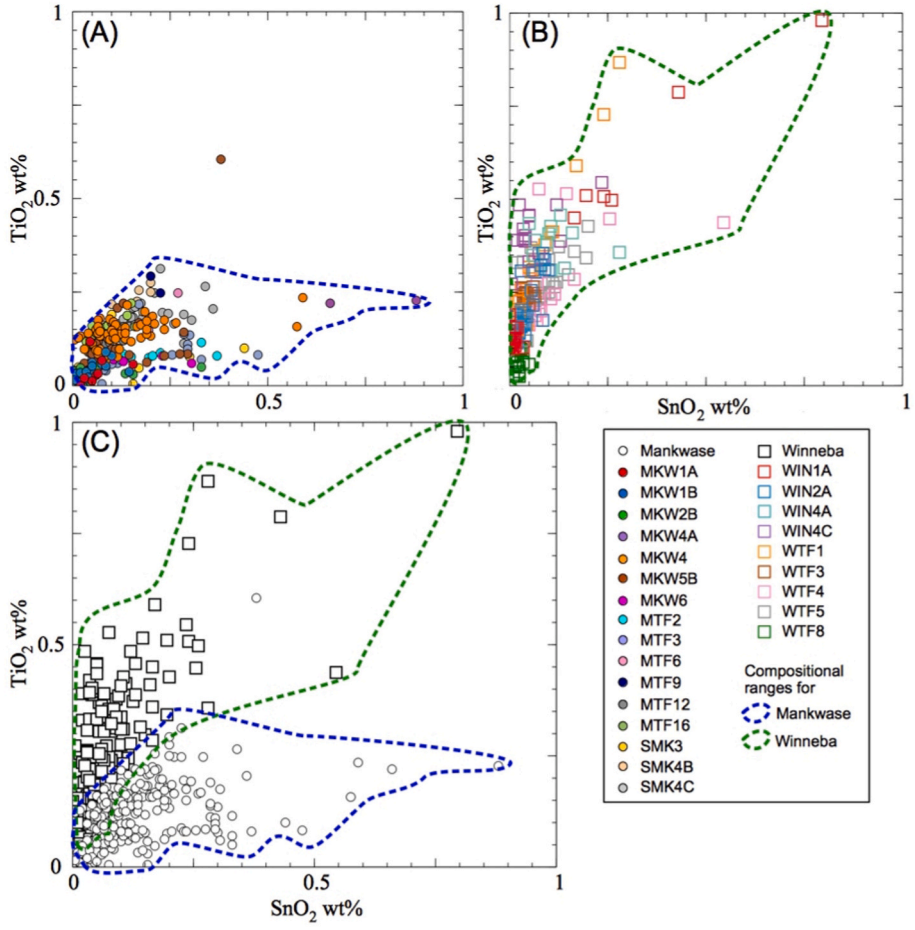


**Fig. 11.** Ti versus Sn concentrations of CGM for Mankoadze (A), Winneba (B) and comparison of the two compositional fields (C).

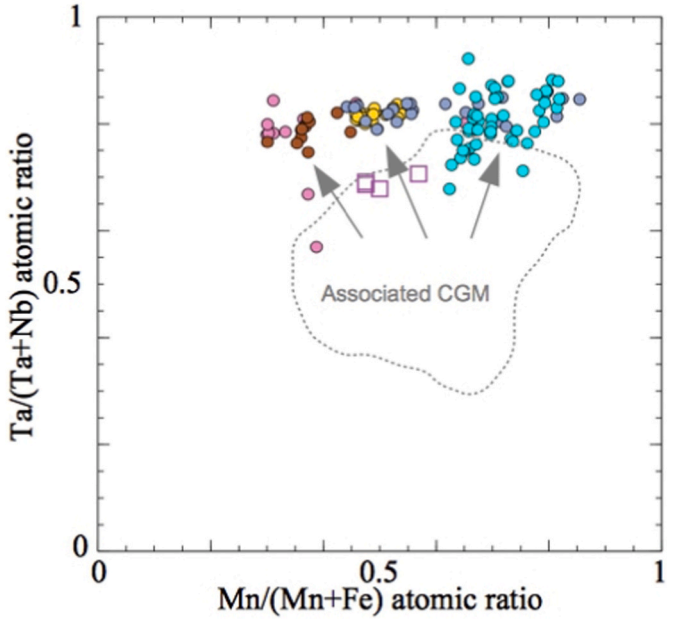


**Fig. 12.** Composition of WGM in the columbite quadrilateral, also showing the compositional field of the CGM associated in the same sample. Same labels as in Fig. 10.

Rayleigh-type Fe/Mn fractionation at Winneba and Mankoadze, with Fe/Mn atomic ratios below 1.5. This value is comparable to the garnet of the complex rare-element spodumene-subtype Kenticha pegmatite with Fe/Mn ratios below 1 (Bekele and Sen, 2020). In conclusion, the Winneba and Mankoadze minerals show a degree of fractionation that is comparable to that of the most fractionated pegmatites in the world.

The varying mineral fractionation allows the construction of a general pattern of differentiation inside each pegmatite field (Fig. 14). At Mankoadze, the highest $Rb_2O$ values in micas occur at outcrop MKW2. Although there are only two analyses in MKW6, they also fall into the most fractionated compositions. The least fractionated mica compositions are found at outcrops MTF9 and MKW7. In sample MTF11 of the MTF9 outcrop, mica is included in spodumene. This textural evidence of its primary magmatic origin attests to the fact that the mica composition reflects the primary magmatic processes of the melt evolution. In the CGM and WGM, the most fractionated compositions are those with the highest Ta/(Ta + Nb) and Mn/(Mn + Fe) ratios. They occur at outcrops MKW1, MKW2, and MKW6 in the Mankoadze area. The degree of fractionation of garnet between the different samples does not enable the drawing of a general fractionation pattern; at Mankoadze, the most and least fractionated garnets occur in proximal outcrops. In conclusion, a general pattern of differentiation appears to be in a SE-NW direction (Fig. 14).

At Winneba, the least fractionated mica occurs in WTF1, which is the southernmost outcrop. The most fractionated CGM, WGM and garnet compositions occur in the center of the pegmatite field. For eight samples, it is possible to correlate the Fe/Mn ratios of coexisting garnet and CGM (Fig. 15). The diagram shows a positive correlation between both fractionation indicators. This is evidence that the two minerals are

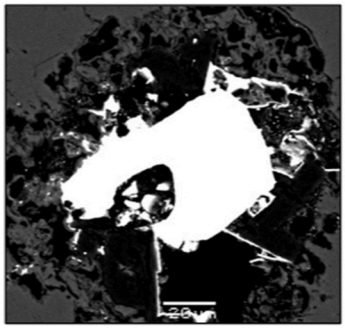

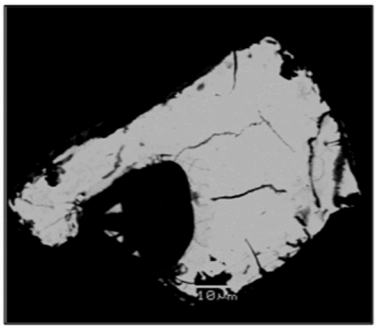

| | |
|---|---|
| Nb2O5 | 0.44 |
| Ta2O5 | 70.78 |
| MnO | 0.52 |
| FeO | 0.57 |
| Na2O | 0.00 |
| CaO | 0.00 |
| SnO2 | 0.13 |
| WO3 | 0.00 |
| TiO2 | 0.10 |
| PbO | n.a. |
| ThO2 | n.a. |
| UO2 | 13.50 |
| Total | 86.04 |

**Fig. 13.** Unidentified U–Ta-bearing mineral in BSE imaging, with EPMA composition of the shown crystal in wt%. Sample MKW2B.

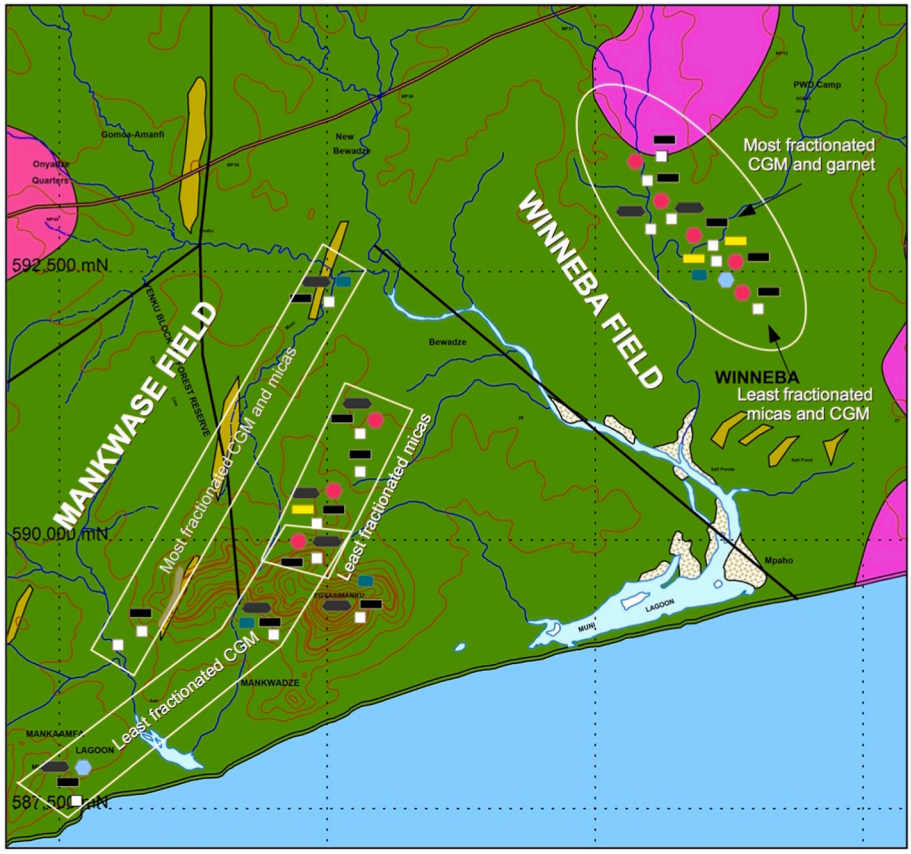


**Fig. 14.** Lithological map showing the pegmatite mineral distribution and principal fractionation trends.

primarily magmatic in origin and that their Fe–Mn composition is controlled by magmatic fractionation. Both minerals then show increasing fractionation from the southernmost part to the central part of the pegmatite field.

These distinct differentiation patterns between the studied areas are further evidence that the two pegmatite groups are distinct fields that evolved independently and may have different origins.

### 5.4. Emplacement of the pegmatites

MKW1, MKW2, and MKW6 host the most Cs-rich micas together with the most evolved manganotantalite compositions. They could represent the most evolved degree of fractionation of the pegmatite melt. However, they occur a few meters away from ultramafic dykes. These cold and refractory rocks could have acted as traps next to which the pegmatite-forming melt cooled more rapidly than in the gneissic and amphibolitic country rocks, leading to stronger undercooling and rare-metal fractionation (Van Lichtervelde et al., 2006, 2018). This is consistent with the fine-grained albitic texture, similar to that of aplite, found in outcrops MKW1 and MKW2 (Fig. 4A). Preliminary back-scattered electron images also reveal oscillatory zoning in the CGM in MKW6 and MKW1B, accompanied by strong Nb–Ta fractionation, which is interpreted as the result of strong undercooling (Van Lichtervelde et al., 2018). This interpretation implies that most fractionated pegmatite samples do not necessarily result from liquid differentiation, but rather reflect different crystallization kinetics.

The U–Ta-rich metamict phase is considered as a late, possibly secondary hydrothermal phase. Its presence could reflect the interaction of U-bearing fluids with the pegmatite-forming melt during late-stage crystallization. Another explanation is that it could reflect a U-rich pegmatite-forming melt in which uranium behaved incompatibly and was concentrated in late-stage liquid until it precipitated as late primary U–Ta-rich minerals (Cuney, 2014). In any case, this mineral attests the strongly U-rich environment in which the Winneba-Mankoadze

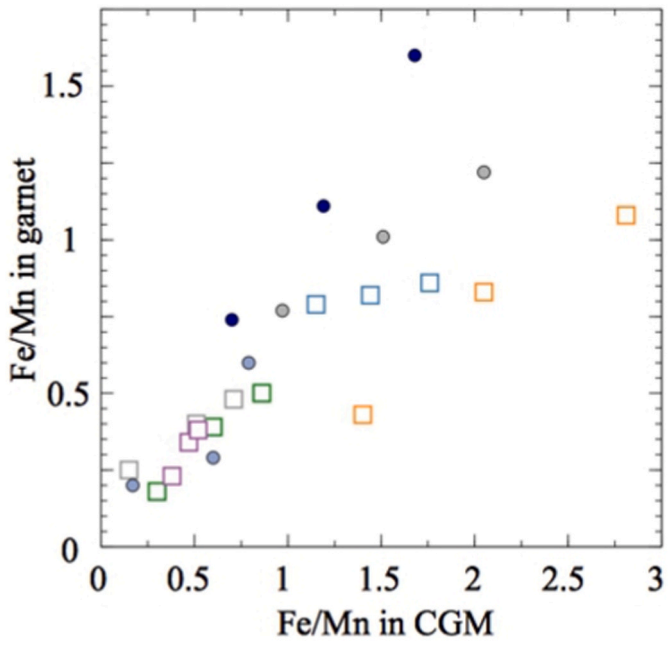


**Fig. 15.** Comparison of the Fe/Mn atomic ratios (minimum, maximum and average ratios for each sample) between coexisting garnet and CGM. Same labels as in Fig. 9.

pegmatites were emplaced.

### 5.5. Origin of the Winneba-Mankoadze pegmatites

The Winneba granite was dated at 2139 ± 6 Ma by Petersson et al. (2018) and outcrops about 20 km away from the studied area. The pegmatites at Winneba-Mankoadze were not dated, but preliminary U–Pb ages on the CGM (unpublished data from the second author) display results in the range of other LCT pegmatites in the West-African Craton, dated around 2080–2050 Ma in various localities (Melcher et al., 2008; Legros et al., 2019). If the CGM ages at Winneba-Mankoadze are confirmed, the Winneba granite would be too old to be the source of the LCT pegmatites. Therefore, the Winneba-Mankoadze pegmatites cannot be interpreted as a single pegmatite field that evolved with fractionation from the north-east to the south-west away from the Winneba granite source. A large area that extends between Winneba and Cape Coast, ~90 km to the west, hosts other pegmatite fields that are not associated with peraluminous granites, and their origin is as yet unknown. The granitic origin of the pegmatites can therefore be questioned. Among others, Knoll et al. (2023) have shown that albite-spodumene rare-element pegmatites of the Austroalpine Province probably originated from the anatexis of staurolite-bearing metapelites. Mica schists do not occur in the Winneba-Mankoadze area, but staurolite is found in abundance in the soils covering the top of the Ewoyaa lithium pegmatite deposit, currently under exploration (in 2022), located 50 km to the west of Winneba. Consequently, an anatectic origin involving the melting of lithium-rich metasedimentary sources, with lithium being hosted by staurolite, has to be considered.

The mineral fractionation patterns in the studied pegmatites provide evidence for the independent formation and evolution of the two pegmatite fields. The micas at Winneba are ten times richer in Ti and Mg than the Mankoadze micas, and this enrichment is not correlated with the fractionation degree. Similarly, the garnet Mg content at Winneba is much higher than at Mankoadze, and MgO shows different correlation trends with the Fe/Mn fractionation indicator (Fig. 9B). For the CGM, the Ti versus Sn diagram is clearly discriminant between the two areas. Consequently, the minor element chemistry of these accessory minerals could reflect the different minor element geochemistry of the pegmatite-forming melts, which is not related to fractional crystallization but rather relates to chemically heterogeneous anatectic sources. In particular, the high Ti content of the CGM is the signature of abundant lithium mineralization, such as that observed at Winneba. This opens new opportunities to fingerprint Li mineralization in pegmatites using the minor element geochemistry of Nb–Ta–Sn oxides.

## 6. Conclusions

The Winneba-Mankoadze area offers the opportunity to study highly differentiated, strongly mineralized pegmatites of the LCT family and albite-spodumene type along the coast between Accra and Cape Coast in southern Ghana. Fractionation indicators in micas, garnet, and Nb–Ta–Sn oxides reveal fractionation levels comparable to the most evolved pegmatites worldwide. In particular, extreme Nb–Ta fractionation is observed in columbite-group minerals in close proximity to ultramafic rocks, which is a common feature of strongly mineralized LCT pegmatites worldwide.

The field relationships and mineral characteristics argue for two distinct pegmatite fields that evolved independently and may have originated from the partial melting of chemically heterogeneous staurolite-bearing metasedimentary rocks. The accessory mineral geochemistry registered these heterogeneities and can be used as a tool to discriminate Li-mineralized pegmatites. Finally, the study area offers the opportunity to investigate particularly complex accessory mineral assemblages, including Nb–Ta–Sn oxides, phosphates, and U–Th minerals, which are important to drive rare metal exploration in pegmatites.

## Declaration of competing interest

The authors declare that they have no known competing financial interests or personal relationships that could have appeared to influence the work reported in this paper.

## Data availability

Data will be made available on request.

## Acknowledgements

The first author benefited from a fellowship through the Exchange Program of the French Institut de Recherche pour le Développement (IRD) for the laboratory work. The laboratory analyses (petrography, SEM, and EMPA) were done at the Géosciences Environnement Toulouse (GET) Laboratory of the University of Toulouse III (Paul Sabatier), France. We thank T. Aigouy, P. De Parseval, and S. Gouy for their assistance in using the SEM and EPMA equipments.

## Appendix A. Supplementary data

Supplementary data to this article can be found online at https://doi.org/10.1016/j.jafrearsci.2023.105049.

## References

Adams, S.J., 2013. Rare-metal Mineralization of the Winneba-Mankwase Pegmatites, Southwestern Ghana. Graduate School of Nuclear and Allied Sciences, University of Ghana, pp. 1–101. MPhil Thesis.

Agomor, A.K., 1987. Geological indications and prospecting guide to rare metal mineralisation of birimian granite pegmatite of Ghana. In: Proceeding of the International Conference on the Geology of Ghana with Emphasis on Gold, vol. 1. Geological Survey Department, Accra, Ghana. B-2–B-24.

Agyei-Duodu, J., Loh, G.K., Boamah, K.O., Baba, M., Hirdes, W., Toloczyki, M., Davis, D. W., 2009. Geological Survey Department of Ghana (GSD) Report, vol. 1. Geological Map of Ghana, Accra Ghana, 1000000.

Allou, A.B., 2005. Facteurs, paramètres, dynamique de distribution et genèse des dépôts de columbo-tantalite d'Issia, centre-ouest de la Côte d'Ivoire. Université du Québec à Chicoutimi, p. 352. Canada, Thèse.

Allou, A.B., Lu, H.-Z., Guha, J., Carignan, J., Naho, J., Pothin, K., Yobou, R., 2005. Une Corrélation Génétique entre les Roches Granitiques, et les Dépôts Éluvionnaires, Colluvionnaires et Alluvionnaires de Columbo-Tantalite d'Issia, Centre-Ouest de la Côte d'Ivoire. Explor. Min. Geol. 14 (1–4), 61–77.
Amponsah, P.O., Salvi, S., Didier, B., Baratoux, L., Siebenaller, L., Jessell, M., Nude, P.M., Gyawu, E.A., 2016a. Multistage gold mineralization in the Wa-Lawra greenstone belt, NW Ghana: the Bepkong deposit. J. Afr. Earth Sci. 120, 220–237.
Amponsah, P.O., Salvi, S., Béziat, D., Baratoux, L., Siebenaller, L., Nude, P.M., et al., 2016b. The Bepkong gold deposit, northwestern Ghana. Ore Geol. Rev. 78, 718–723.
Amponsah, P.O., Salvi, S., Béziat, D., Siebenaller, L., Baratoux, L., Jessell, M.W., 2015. Geology and geochemistry of the shear-hosted Julie gold deposit, NW Ghana. J. Afr. Earth Sci. 112, 505–523.
Amponsah, P.O., 2012. Multiscale Structural Analysis of the Sunyani Basin, Ghana. Unpublished MSc Thesis, Department of Earth Science, University of Ghana.
Anum, S., Sakyi, P.A., Su, B.X., Nude, P.M., Nyame, F., Asiedu, D., Kwayisi, D., 2015. Geochemistry and geochronology of granitoids in the Kibi-Asamankese area of the Kibi-Winneba volcanic belt, southern Ghana. J. Afr. Earth Sci. 102, 166–179.
Asiedu, D.K., Agoe, M., Amponsah, P.O., Nude, P.M., Anani, C.Y., 2019. Geochemical constraints on provenance and source area weathering of metasedimentary rocks from the Paleoproterozoic (~ 2.1 Ga) Wa-Lawra Belt, southeastern margin of the West African Craton. Geodin. Acta 31 (1), 27–39.
Baldwin, J.R., von Knorring, O., 1983. Compositional range of Mn-garnet in zoned granitic pegmatites. Can. Mineral. 21 (4), 683–688.
Ballouard, C., Poujol, M., Boulvais, P., Branquet, Y., Tartèse, R., Vigneresse, J.L., 2016. Nb-Ta fractionation in peraluminous granites: a marker of the magmatic-hydrothermal transition. Geology 44, 231–234.
Bekele, B., Sen, A.K., 2020. The mineral chemistry of gahnite, garnet and columbite-group minerals (CGM): implications for genesis and evolution of the Kenticha Rare-element granite-pegmatite, Adola, Ethiopia. J. Afr. Earth Sci. 162, 103691.
Block, S., Jessell, M., Ailleres, L., Baratoux, L., Bruguier, O., Zeh, A., Bosch, D., Caby, R., Mensah, E., 2016. Lower crust exhumation during Paleoproterozoic (Eburnean) orogeny, NW Ghana, West African Craton: interplay of coeval contractional deformation and extensional gravitational collapse. Precambrian Res. 274, 82–109.
Bonzi, W.M.-E., Van Lichtervelde, M., Vanderhaeghe, O., André-Mayer, A.-S., Salvi, S., Wenmenga, U., 2022. Insights from mineral trace chemistry on the origin of NYF and mixed LCT + NYF pegmatites and their mineralization at Mangodara, SW Burkina Faso. Miner. Deposita 58, 75–104.
Černý, P., 1989. Characteristics of pegmatite deposits of tantalum. In: Lanthanides, Tantalum and Niobium: Mineralogy, Geochemistry, Characteristics of Primary Ore Deposits, Prospecting, Processing and Applications Proceedings of a Workshop in Berlin. Springer Berlin Heidelberg, pp. 195–239. November 1986.
Černý, P., 1991. Rare-element granitic pegmatites. Part I: anatomy and internal evolution of pegmatite deposits. Geosci. Can. 18 (2), 49–67.
Černý, P., Ercit, T.S., 1989. Mineralogy of niobium and tantalum: crystal chemical relationships, paragenetic aspects and their economic implications. In: Lanthanides, Tantalum and Niobium: Mineralogy, Geochemistry, Characteristics of Primary Ore Deposits, Prospecting, Processing and Applications Proceedings of a Workshop in Berlin. Springer Berlin Heidelberg, pp. 27–79. November 1986.
Černý, P., Ercit, T.S., 2005. The classification of granitic pegmatites revisited. Can. Mineral. 43 (6), 2005–2026.
Černý, P., Meintzer, R.E., Anderson, A.J., 1985. Extreme fractionation in rare-element granitic pegmatites; selected examples of data and mechanisms. Can. Mineral. 23 (3), 381–421.
Chalokwu, C.I., Ghazi, M.A., Foord, E.E., 1997. Geochemical characteristics and K- Ar ages of rare-metal bearing pegmatites from the Birimian of southeastern Ghana. J. Afr. Earth Sci. 24 (1–2), 1–9.
Cuney, M., 2014. Felsic magmatism and uranium deposits. Bull. Soc. Geol. Fr. 185, 75–92.
Dampare, S.B., Nyarko, B.J.B., Osae, S., Akaho, E.H.K., Asiedu, D.K., Serfor-Armah, Y., Nude, P., 2005. Simultaneous determination of tantalum, niobium, thorium and uranium in placer columbite-tantalite deposits from the Akim Oda District of Ghana by epithermal instrumental neutron activation analysis. J. Radioanal. Nucl. Chem. 265 (1), 53–59.
Dill, H.G., 2015. Pegmatites and aplites: their genetic and applied ore geology. Ore Geol. Rev. 69, 417–561.
Feng, X., Wang, E., Amponsah, P.O., Ganne, J., Martin, R., Jessell, M.W., 2019. Effect of pre-existing faults on the distribution of lower crust exhumation under extension: numerical modelling and implications for NW Ghana. Geosci. J. 23, 961–975.
Feng, X., Jessell, M.W., Amponsah, P.O., Martin, R., Ganne, J., Liu, D., Batt, G.E., 2016. Effect of strain-weakening on Oligocene–Miocene self-organization of the Australian-Pacific plate boundary fault in southern New Zealand: insights from numerical modelling. J. Geodyn. 100, 130–143.
Fetherston, J.M., 2004. Tantalum in western Australia. Miner. Resour. Bull. Geol. Surv. West Aust. 22, 1–162.
Forson, E.D., Amponsah, P.O., Hagan, G.B., Sapah, M.S., 2023. Frequency ratio-based flood vulnerability modeling over the greater Accra Region of Ghana. Modeling Earth Syst. Environ. 9 (2), 2081–2100.
Forson, E.D., Menyeh, A., Wemegah, D.D., Danuor, S.K., Adjovu, I., Appiah, I., 2020. Mesothermal gold prospectivity mapping of the southern Kibi-Winneba belt of Ghana based on Fuzzy analytical hierarchy process, concentration-area (CA) fractal model and prediction-area (PA) plot. J. Appl. Geophys. 174, 103971.
Hernández-Filiberto, L., Roda-Robles, E., Simmons, W.B., Webber, K.L., 2021. Garnet as indicator of pegmatite evolution: the case study of pegmatites from the Oxford pegmatite field (Maine, USA). Minerals 11 (8), 802.
Hirdes, W., Davis, D.W., Eisenlohr, B.N., 1992. Reassessment of Proterozoic granitoid ages in Ghana on the basis of U/Pb zircon and monazite dating. Precambrian Res. 56 (1–2), 89–96.
Hulsbosch, N., Hertogen, J., Dewaele, S., André, L., Muchez, P., 2014. Alkali metal and rare earth element evolution of rock-forming minerals from the Gatumba area pegmatites (Rwanda): quantitative assessment of crystal-melt fractionation in the regional zonation of pegmatite groups. Geochem. Cosmochim. Acta 132, 349–374.
Jessell, M.W., Amponsah, P.O., Baratoux, L., Asiedu, D.K., Loh, G.K., Ganne, J., 2012. Crustal-scale transcurrent shearing in the paleoproterozoic Sefwi-Sunyani-Comoe region, West Africa. Precambrian Res. 212, 155–168.
Kesse, G.O., 1985. The Mineral and Rock Resources of Ghana. Balkema, Rotterdam, p. 610.
Knoll, T., Huet, B., Schuster, R., Mali, H., Ntaflos, T., Hauzenberger, C., 2023. Lithium pegmatite of anatectic origin-A case study from the Austroalpine Unit Pegmatite Province (Eastern European Alps): geological data and geochemical model. Ore Geol. Rev. 105–298.
Koffi Brou, J., Van Lichtervelde, M., Kouamelan, N.A., Baratoux, D., Thébaud, N., 2022. Petrogenetic relationships between peraluminous granites and Li- Cs-Ta rich pegmatites in south Issia zone (Central-West of Côte d'Ivoire): petrography, Mineralogy, Geochemistry and zircon U–Pb Geochronology. Mineral. Petrol. 116, 443–471.
Küster, D., Romer, R.L., Tolessa, D., Zerihun, D., Bheemalingeswara, K., Melcher, F., Oberthür, T., 2009. The Kenticha rare-element pegmatite, Ethiopia: internal differentiation, U–Pb age and Ta mineralization. Miner. Deposita 44, 723–750.
Legros, H., Mercadier, J., Villeneuve, J., Romer, R.L., Deloule, E., Van Lichtervelde, M., Dewaele, S., Lach, P., et al., 2019. U-Pb isotopic dating of columbite-tantalite minerals: development of reference materials and in situ applications by ion microprobe. Chem. Geol. 512, 69–84.
Leube, A., Hirdes, W., Mauer, R., Kesse, G.O., 1990. The early Proterozoic Birimian Supergroup of Ghana and some aspects of its associated gold mineralization. Precambrian Res. 46 (1–2), 139–165.
Linnen, R.L., Van Lichtervelde, M., Černý, P., 2012. Granitic pegmatites as sources of strategic metals. Elements 8, 275–280.
Linnen, R.L., Keppler, H., 1997. Columbite solubility in granitic melts: consequences for the enrichment and fractionation of Nb and Ta in the Earth's crust. Contrib. Mineral. Petrol. 128 (2–3), 213–227.
Linnen, R.L., Van Lichtervelde, M., Černý, P., 2012. Granitic pegmatites as sources of strategic metals. Elements 8 (4), 275–280.
Llorens, T., Moro, M.C., 2012. Oxide minerals in the granitic cupola of the Jálama Batholith, Salamanca, Spain. Part I: accessory Sn, Nb, Ta and Ti minerals in leucogranites, aplites and pegmatites. J. Geosci. 57 (1), 25–43.
London, D., 1987. Internal differentiation of rare-element pegmatites: effects of boron, phosphorus and fluorine. Geochem. Cosmochim. Acta 51, 403–420.
London, D., 2014. A petrologic assessment of internal zonation in granitic pegmatites. Lithos 184, 74–104.
London, D., Morgan, G.B., 2017. Experimental crystallization of the Macusani obsidian, with applications to lithium-rich granitic pegmatites. J. Petrol. 58 (5), 1005–1030.
Manning, D.A.C., 1983. Chemical variation in garnets from aplites and pegmatites, peninsular Thailand. Mineral. Mag. 47 (344), 353–358.
Melcher, F., Sitnikova, M.A., Graupner, T., Martin, N., Oberthür, T., Henjes-Kunst, F., et al., 2008. Fingerprinting of conflict minerals: columbite-tantalite ("coltan") ores. Sga News 23 (1), 7–14.
Melcher, F., Graupner, T., Gäbler, H.E., Sitnikova, M., Henjes-Kunst, F., Oberthür, T., Gerdes, A., Dewaele, S., 2015. Tantalum–(niobium–tin) mineralisation in African pegmatites and rare metal granites: constraints from Ta–Nb oxide mineralogy, geochemistry and U–Pb geochronology. Ore Geol. Rev. 64, 667–719.
Milesi, J.P., Feybesse, J.L., Pinna, P., Deschamps, Y., Kampunzu, H., Muhongo, S., Lescuyer, J.L., Le Goff, E., Delor, C., Billa, M., Ralay, F., Heinry, C., 2004. Geological map of Africa 1:10,000,000, SIGAfrique project. In: 20th Conference of African Geology, BRGM, Orleans, France, 2–7 June.
Ndiaye, P.M., Dia, A., Vialette, Y., Diallo, D., Ngom, P., Sylla, M., Wade, S., Dioh, E., 1997. Données pétrographiques, géochimiques et géochronologiques nouvelles sur les granitoïdes du Paléoprotérozoïque du Supergroupe de Dialé-Daléma (Sénégal Oriental): implications pétrogénétiques et géodynamiques. J. Afr. Earth Sci. 25 (2), 193–208.
Nude, P.M., Hanson, J.E.K., Dampare, S.B., Akiti, T.T., Osae, S., Nyarko, E.S., Zakaria, N., Enti-Brown, S., 2011. Geochemistry of Pegmatites associated with the cape coast granite complex in the Egyaa and Akim Oda areas of southern Ghana. Ghana J. Sci. 51, 89–100.
Nyame, F.K., Armah, T.K., Ibrahim, K., Baah-Acheamfour, J., Manu, J., Tigme, J., 2021. Manganese occurrence in the Mankwadzi Area, southern Kibi–Winneba metavolcanic belt, Ghana: typical or atypical palaeoproterozoic Birimian Mn mineralization? Geol. Soc., London, Special Publ. 502 (1), 331–348.
Petersson, A., Scherstén, A., Kemp, A.I., Kristinsdóttir, B., Kalvig, P., Anum, S., 2016. Zircon U–Pb–Hf evidence for subduction related crustal growth and reworking of Archaean crust within the Palaeoproterozoic Birimian terrane, West African Craton, SE Ghana. Precambrian Res. 275, 286–309.
Petersson, A., Scherstén, A., Gerdes, A., 2018. Extensive reworking of Archaean crust within the Birimian terrane in Ghana as revealed by combined zircon U-Pb and Lu-Hf isotopes. Geosci. Front. 9 (1), 173–189.
Pouchou, J.L., Pichoir, F., 1985. "PAP" procedure for improved quantitative micro-analysis. Microbeam Anal. 20, 104–105.
Roda Robles, E., Pesquera, A., Gil-Crespo, P.P., Torres-Ruiz, J., De Parseval, P., 2006. Mineralogy and geochemistry of micas from the Pinilla de Fermoselle pegmatite (Zamora, Spain). Eur. J. Mineral 18 (3), 369–377.

Rudnick, R.L., Gao, S., 2003. Composition of the continental crust. Treatise Geochem. 3, 659.
Salvi, S., Amponsah, P.O., Siebenaller, L., Béziat, D., Baratoux, L., Jessell, M., 2016. Shear-related gold mineralization in Northwest Ghana: the Julie deposit. Ore Geol. Rev. 78, 712–717.
Sakyi, P.A., Manu, J., Su, B.X., Kwayisi, D., Nude, P.M., Dampare, S.B., 2019. Geochemical and Sm–Nd isotopic evidence for the composition of the palaeoproterozoic crust of the West african craton in Ghana. Geol. J. 54 (6), 3940–3957.
Sapah, M.S., Agbetsoamedo, J.E., Amponsah, P.O., Dampare, S.B., Asiedu, D.K., 2021. Neodymium isotope composition of palaeoproterozoic birimian shales from the wa-lawra belt, north-west Ghana: constraints on provenance. Geol. J. 56 (4), 2072–2081.
Taylor, P.N., Moorbath, S., Leube, A., Hirdes, W., 1992. Early Proterozoic crustal evolution in the Birimian of Ghana: constraints from geochronology and isotope geochemistry. Precambrian Res. 56 (1–2), 97–111.
Tindle, A.G., Breaks, F.W., 2000. Columbite-tantalite mineral chemistry from rare-element granitic pegmatites: separation Lakeh area, NW Ontario, Canada. Mineral. Petrol. 70 (3/4), 165.
Thomas, R., Davidson, P., 2007. The Formation of Granitic Pegmatites from the Viewpoint of Melt and Fluid Inclusions and New Experimental Work. Granitic Pegmatites: the State of the Art, Book of Abstracts, Dep. Geologia FCUP, Porto, Portugal, pp. 13–16.
Tischendorf, G., Gottesmann, B., Foerster, H.J., Trumbull, R.B., 1997. On Li-bearing micas: estimating Li from electron microprobe analyses and an improved diagram for graphical representation. Mineral. Mag. 61 (409), 809–834.
Van Lichtervelde, M., Linnen, R.L., Salvi, S., Beziat, D., 2006. Evaluating the role of metagabbro rafts on tantalum mineralisation in the Tanco pegmatite, Manitoba. Can. Mineral. 44, 625–644.
Van Lichtervelde, M., Grégoire, M., Linnen, R.L., Béziat, D., Salvi, S., 2008. Trace element geochemistry by laser ablation ICP-MS of micas associated with Ta mineralization in the Tanco pegmatite, Manitoba, Canada. Contrib. Mineral. Petrol. 155, 791–806.
Van Lichtervelde, M., Holtz, F., Melcher, F., 2018. The effect of disequilibrium crystallization on Nb-Ta fractionation in pegmatites: constraints from crystallization experiments of tantalite-tapiolite. Am. Mineral. 103 (9), 1401–1416.
Von Knorring, O., Condliffe, E., 1987. Mineralized pegmatites in Africa. Geol. J. 22 (S2), 253–270.
Whitney, D.L., Evans, B.W., 2010. Abbreviations for names of rock-forming minerals. Am. Mineral. 95 (1), 185–187.
Wilde, A., Otto, A., McCracken, S., 2021. Geology of the Goulamina spodumene pegmatite field, Mali. Ore Geol. Rev. 134, 104–162.
Yao, Y., Robb, L.J., 1998. The Birimian Granitoids of Ghana: A Review. Information Circular 322. University of the Witwatersrand, Economic Geology Research Unit, Johannesburg, p. 46.